FINITE ELEMENT ANALYSES OF PATHOLOGICAL CHANGES IN THE LUMBAR VERTEBRAL BODY

by

Peter Condax

SUBMITTED TO THE DEPARTMENT OF MECHANICAL ENGINEFRING IN PARTIAL FULFILLMENT OF THE REQUIREMENTS FOR THE DEGREE OF

BACHELOR OF SCIENCE

at the

MASSACHUSETTS INSTITUTE OF TECHNOLOGY

June 1990

Signature of Author ______________________
Department of Mechanical Engineering
June 4, 1990

Certified by ______________________
Professor Wilson C. Hayes
Thesis Supervisor

Certified by ______________________
Professor Joe Mizrahi
Thesis Supervisor

Accepted by ______________________
Professor Peter C. Griffith
Chairman, Undergraduate Thesis Committee

FINITE ELEMENT ANALYSES OF PATHOLOGICAL CHANGES IN THE LUMBAR VERTEBRAL BODY

by

Peter Condax

Submitted to the Department of Mechanical Engineering on June 4, 1990 in partial fulfillment of the requirements for the degree of Bachelor of Science.

Abstract

This project aimed in the finite element modeling of a vertebral body and in particular the modeling of osteoporosis and of metastatic defects. The geometric considerations included tapering, teardrop cross sectional geometry as well as biconcavity of the endplate. The improvement in modeling by the utilization of more realistic property data derived by regional QCT density measurements was also examined and evaluated. Osteoporosis was modeled as a reduction in the mechanical properties of both cancellous and cortical bone. The parametric study of the effects of a metastatic defect was done by defining two parameters related to its position and size. The case in which both cancellous and cortical bone were degenerated due to a metastatic defect was also considered.

The criteria with which results were examined and compared were nodal displacement, principal stress and Von Mises stress. In particular, Von Mises stress was determined to be the most important criteria, because of its capacity to describe the stress state at a point with a scalar, non vectorial or tensorial, quantity. The results demonstrated that the utilization of variable regional densities did not significantly change the mechanical behavior of the model. The consideration of biconcavity, however, altered substantially the mechanical behavior and was found to be necessary in order for an accurate model to be produced. Osteoporosis was found to have relatively strong influence in causing peak displacements to rise to values up to 67% and principal stresses up to 47%. For the metastatic defect case size was found to be the most critical parameter (stresses were higher by 300% for a doubling in the diameter of the spherical defect) but also location influenced the mechanical behavior although no clear trend was found to correlate location and change in mechanical behavior. Finally, the metastatic defect that penetrated the anterior cortex was found to also strongly influence the mechanical behavior of the vertebral body, especially in the case of non-uniform pressure loading in which peak principal stresses were elevated by 93%. The critical regions where failure of the vertebral body would occur first were predicted to be the cortical shell regions directly below the endplate.

Thesis Supervisor: Professor Wilson C. Hayes
Title: Maurice E. Mueller Professor of Biomechanics, Harvard Medical School

Thesis Supervisor: Professor Joe Mizrahi
Title: Visiting Professor, Harvard Medical School

Dedication

Fortunate he who's made the voyage of Odysseus.
Fortunate if on setting out he's felt
the rigging of a love strong in his body,
spreading there like veins where the blood throbs...

And again and again the shade of Odysseus
  appears before me,
  his eyes red from the waves' salt, ...

He is the mighty Odysseus:
  he who proposed the wooden horse
  with which the Achaeans captured Troy.
I imagine he's coming to tell me
  how I too may build a wooden horse
  to capture my own Troy.

He tells me of the harsh pain you feel
  when the ship's sails swell with memory
  and your soul becomes a rudder;
of being alone, dark in the night,
  and helpless as chaff on the threshing floor;...

He speaks...I still see his hands
  that knew how to judge
  the carving of the mermaid at the prow
presenting me the waveless blue sea
                in the heart of winter...

["Reversions on a foreign line of verse" by George Seferis]

Dedicated to all these who made it possible for me to capture my own "Troy".

Dedicated to my parents, grandmother and especially to my brother George, to all my educators and friends.

Dedicated to whom my work will become the "wooden horse" in their search for knowledge.

Table of Contents

Chapter 1

INTRODUCTION

1.1 Spine and Osteoporosis

The spine is the primary mean of the human body to support its weight and absorb the stresses that are produced by the various loading conditions associated with its motion. The spine is a column shaped structure consisting of 29 bones which are arranged as 7 cervical, 12 thoracic, 5 lumbar, and 5 sacrum (Fig. 1) [16]. Each of these "bean" shaped bones is consisted of two areas of distinct properties: an outside hard cortical shell and a porous inner core of cancellous bone(Fig. 2). These two distinct areas have also distinct material properties.

Osteoporosis is a bone disease which is characterized by a loss of bone mass primarily of cancellous bone where the trabeculae become thin and sparse [4] but also of cortical bone. As a result the strength of the bone is reduced and there is an increased susceptibility to fractures. Since the disease is progressive, the elderly have a much higher risk of bone fracture due to osteoporosis. In particular postmenopausal osteoporosis in elderly women is currently a public health problem [6]. Most frequently the fracture of the spine due to spontaneous compressive loading occurs much before the fracture of any other bone, mainly because of the importance of the spine as a supportive structure due to the large magnitude of loads that it supports.

Various treatments exist for osteoporosis such as estrogen replacement therapy . Most of these have serious side effects. The assessment of osteoporosis is mainly done by non-invasively determining the bone density. In such a way bone loss can be determined. Since treatments for osteoporosis have serious side effects a method that would predict the risk of fracture with only inputs the bone geometry and the bone densities would be of major

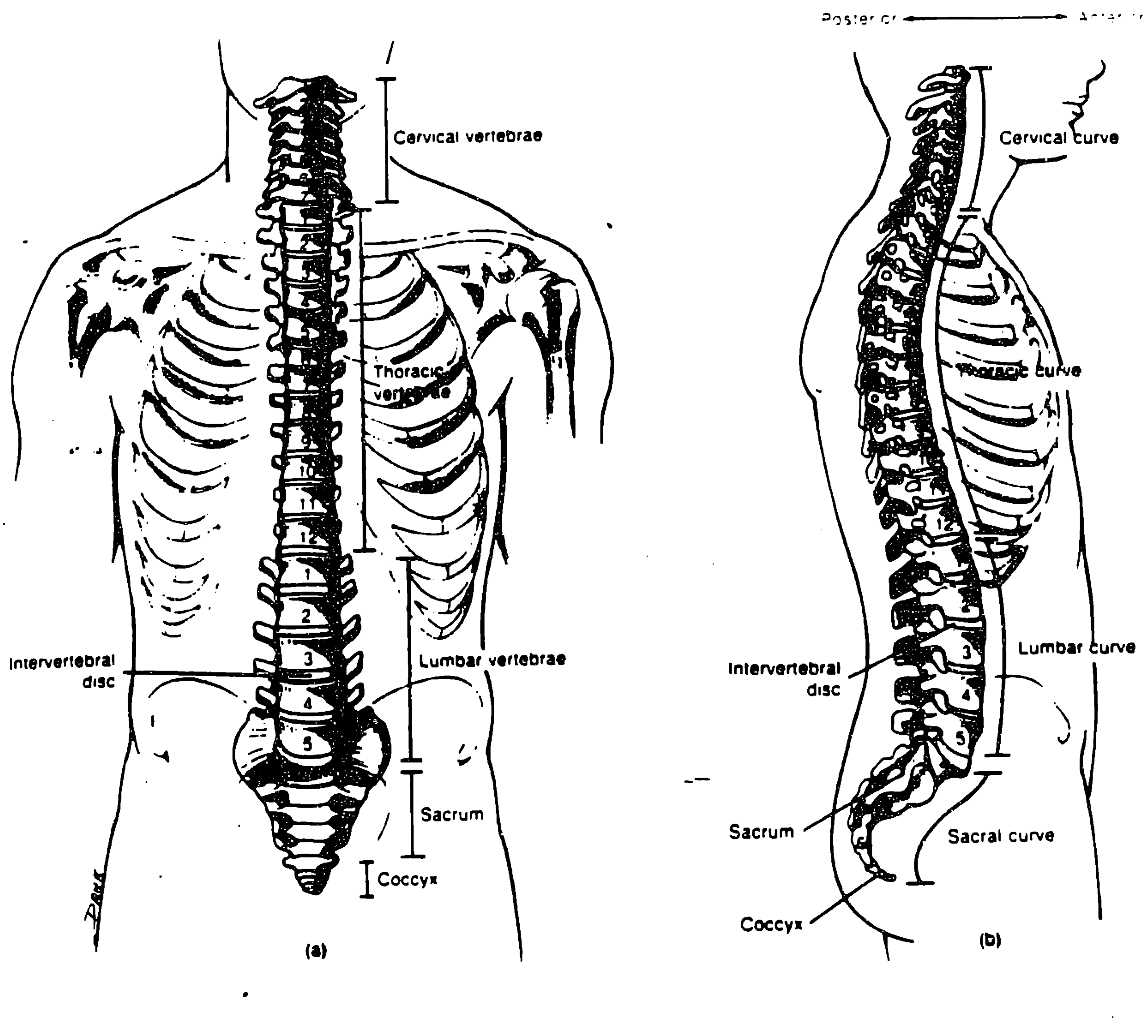

FIGURE 1: THE HUMAN SPINE

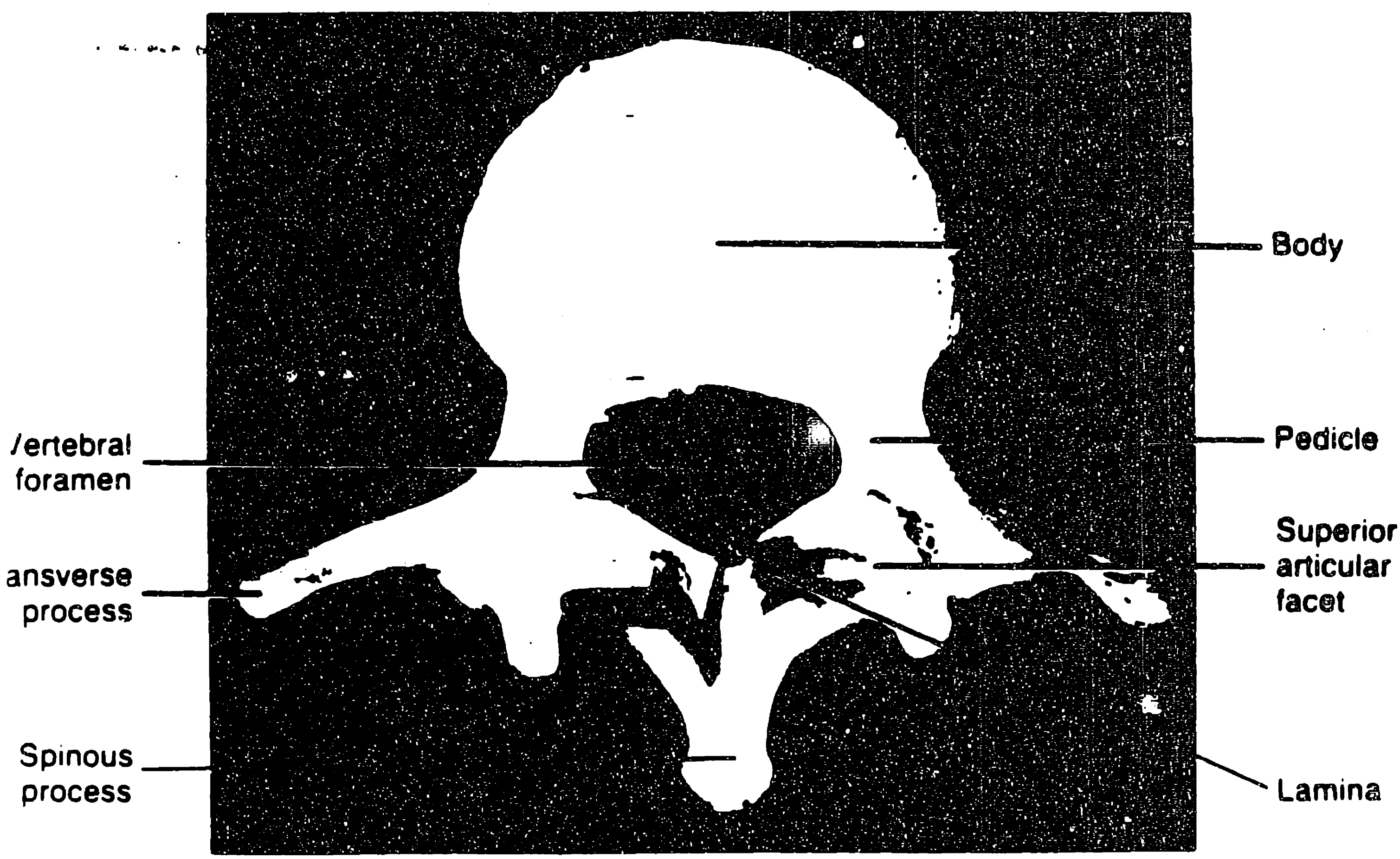

(a)

FIGURE 2: CROSS SECTIONAL GEOMETRY OF A VERTEBRAL BODY

importance. This method would permit a proper assessment of the severity of osteoporosis and the utilization of an effective clinical treatment.

1.2 Quantitative Computed Tomography for the Diagnosis of Osteoporosis

The measurement of bone density is usually performed by non invasive radiographic techniques that accurately determine the mineral bone density. Quantitative Computed Tomography utilizes a bone mineral calibration and has been shown to provide an accurate measurement of spinal cancellous bone density. [7] [17]

1.3 The utilization of Finite Element Methods as a predictive tool

The development of theoretical models for the prediction of mechanical behavior of structures has been largely based on finite element models. Bridges, support structures for buildings and machine parts that support static and cyclic loads are designed by considering finite element methods. These techniques usually require a mathematical expression of the existing geometry and a digital computer for manipulating the input data and producing the output information.

Finite element analysis has been utilized in other studies for the modeling of the in-vivo stress conditions of bone. Knopf [10] developed a finite element model for predicting the strength of a lumbar vertebral body under static compression. Hakim et al [8] who conducted a three-dimensional finite element analysis of a vertebra, with static and dynamic loading patterns, also verified his results experimentally. The same model was further improved by Yang et al [19] by incorporating an adjacent vertebrae and the interconnecting soft tissues. Shirazi et al [18] developed more detailed and technically complex models that reflected the geometry and material properties of normal intact vertebrae based on measurements of vertebral morphology and the material properties of bone and soft tissues.

The above models describe geometry approximations and material properties that vary significantly although most are taken from actual vertebral measurements and testing of bone and soft tissues. The modeling of osteoporosis was not generally considered in previous studies.

1.4 Objectives

The project aimed in the modeling of the centrum of the vertebral body (L3) including the effects of osteoporosis and of metastatic defects. This model could be utilized to predict the static fracture risk in patients with only inputs the individual geometry and bone density data obtained by QCT that can easily be translated into material property data.

Osteoporosis was modeled as a reduction in mechanical properties in both cortical and cancellous bone. A metastatic defect was modeled as a sphere of low Young's modulus that corresponded to bone loss. This spherical volume was placed within the cancellous bone where bone loss most commonly occurs. The contribution of the spherical volume to the mechanical strength of the bone was examined as well as the effects of the change of the location of the sphere within the bone. The metastatic cavity was further placed in the anterior part of the vertebral body in order to model the case in which both cortical and cancellous bone have been affected. A series of 27 models listed in Table 1 was examined examining the effects of variation of material properties and of the geometry.

TABLE 1A : MODELS CREATED

Model #	3	4	5	6	7	8	9	10	11	12	13	14
Uniform Loadcase	Y	N	Y	N	Y	N	Y	N	Y	N	Y	N
Peripheral Loadcase	N	Y	N	Y	N	Y	N	Y	N	Y	N	Y
Ecortical=5,030N/mm^2	Y	Y	Y	Y	Y	Y	Y	Y	Y	Y	N	N
Ecancellous=16.5N/mm^2	Y	Y	N	N	N	N	N	N	N	N	N	N
Variable Ecancellous	N	N	Y	Y	Y	Y	Y	Y	Y	Y	Y	Y
Increased Ecort at the posterior wall	N	N	N	N	Y	Y	Y	Y	Y	Y	Y	Y
Endplate Biconcavity	N	N	N	N	N	N	Y	Y	Y	Y	Y	Y
50% Reduction in Ecanc	N	N	N	N	N	N	N	N	Y	Y	Y	Y
25% Reduction in Ecort	N	N	N	N	N	N	N	N	N	N	Y	Y

TABLE 1B : MODELS CREATED

Model #	15	16	17	18	20	21	22	25	26	27	28	29	30	31	32
Unif.Loadcase	Y	Y	Y	N	N	Y	N	Y	N	Y	N	N	N	N	N
Periph.Loadcase	N	N	N	Y	Y	N	Y	N	Y	N	Y	N	N	N	N
Bending Loadcase	N	N	N	N	N	N	N	N	N	N	N	Y	N	Y	N
Uneven Bend.Loadc.	N	N	N	N	N	N	N	N	N	N	N	N	Y	N	Y
Esphere=10.0N/mm^2	Y	N	N	Y	N	N	N	N	N	N	N	N	N	N	N
Esphere=5.0N/mm^2	N	Y	N	N	N	N	N	N	N	N	N	N	N	N	N
Esphere=0.1N/mm^2	N	N	Y	N	Y	Y	Y	Y	Y	Y	Y	N	N	N	N
Parameter a=0.4	N	N	N	N	N	Y	Y	N	N	N	N	N	N	N	N
Parameter b=0.25	N	N	N	N	N	N	N	Y	Y	N	N	N	N	N	N
Parameter b=0.40	N	N	N	N	N	N	N	N	N	Y	Y	N	N	N	N
Metastatic defect at both cort&canc	N	N	N	N	N	N	N	N	N	N	N	Y	Y	Y	Y
Emetast=0.1N/mm^2	N	N	N	N	N	N	N	N	N	N	N	N	N	Y	Y

Chapter 2

METHODS

2.1 FINITE ELEMENT TOOL PROGRAMS

The strength analysis of the 27 models was performed by the program ADINA a displacement-based element code. The input files for the ADINA program were created by the use of the pre-processor FEMGEN and various pre-ADINA programs. The results were presented and examined using the post-processor FEMVIEW. All programs were run on a DEC VAX/VMS computer system available at the Orthopaedic Biomechanics Laboratory at Beth Israel Hospital.

2.1.1 Material properties

The vertebral body consists of two types of bone: cortical and trabecular or cancellous. Cortical bone is the hard bone that consists the shell and the endplate. The inner part of the vertebral body is consisted by trabecular or cancellous bone that is spongy and soft. In the finite element models used the bone was considered a standard engineering isotropic material. It was characterized by two properties: the modulus of elasticity(Young's modulus,E) and the Poisson's ratio(ν).

2.2 Model Geometry

The geometry of an actual lumbar bone is shown in Fig. 3. In this study only the vertebral body was modeled. Since two planes of symmetry can be assumed in a vertebral body only 1/4 of the body was represented. Since in uniaxial compression most of the load is carried by the vertebral body the elements posterior to the pedicles were removed.

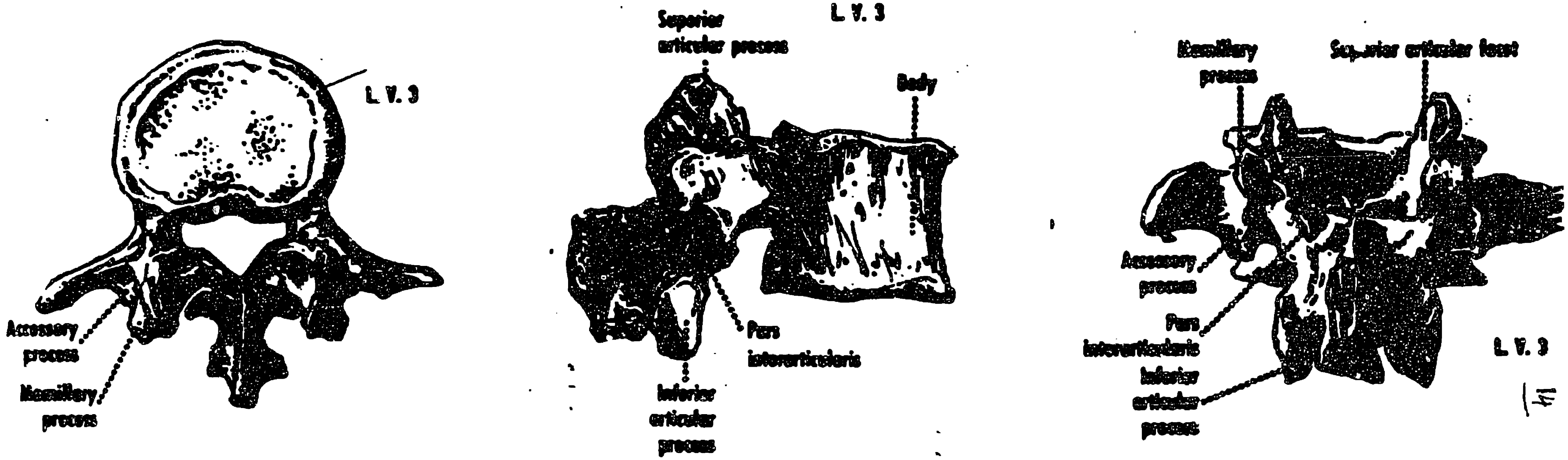

FIGURE 3: A VERTEBRAL BODY

2.2.1 Vertebral Tapering and "Teardrop" Cross Sectional Geometry

The model developed was a quarter of the total vertebral bone and also included the endplate. In actual vertebra the cross sectional area at the center of the bone is less that the one at the endplate and this was taken into account by including tapering in the model.

Since the bodies of actual vertebrae are not exactly cylindrical the geometry produced by the pre-processor FEMGEN had to be modified. The vertebral bodies have the greatest cross-section at the endplate and taper towards the mid-plane. Also the cross sectional geometry is not usually circular but teardrop shaped, often with jagged edges due to the presence of osteophytes.

A program was used [10] (CHANGE 2) in the FORTRAN programming language that changed the geometrical nodal coordinates that were produced by the pre-processor FEMGEN.

The sides of the vertebral body were transformed from straight and vertical to inward sloping curves which were approximated by a cosine function. The taper ratio was set to 0.8 . Also the cross sectional geometry was modified by recalculating the coordinates. The approximation of a teardrop-shaped cross sectional area is as follows:

$$R_i(\phi)=R_{10}(0)[1+0.0063(\cos\phi-2\cos2\phi+\cos3\phi]$$

and was taken from equations originally presented by Broberg [5] to describe the shape of the intervertebral disc. The constant R_{10}=19.9 and 0.0063 were calculated by inputing a saggital diameter of 44.98 and a posterior-anterior diameter of 34.7 as the final dimensions [14] [15]. The height (half of the total height) was taken as 13.95 mm [14] [15]. Figure 4 shows the mesh of the SP2 FEMGEN model. Figures 5, 6 and 7 show the element groups within the vertebral body. The FEMGEN data file for model SP2 is included in the APPENDIX. Also the FORTRAN program CHANGE2 is included in the APPENDIX. [Table 1, Models 3, 4, 5, 6, 7, 8]

JAR FEMGEN 8.0 MODEL : SP2

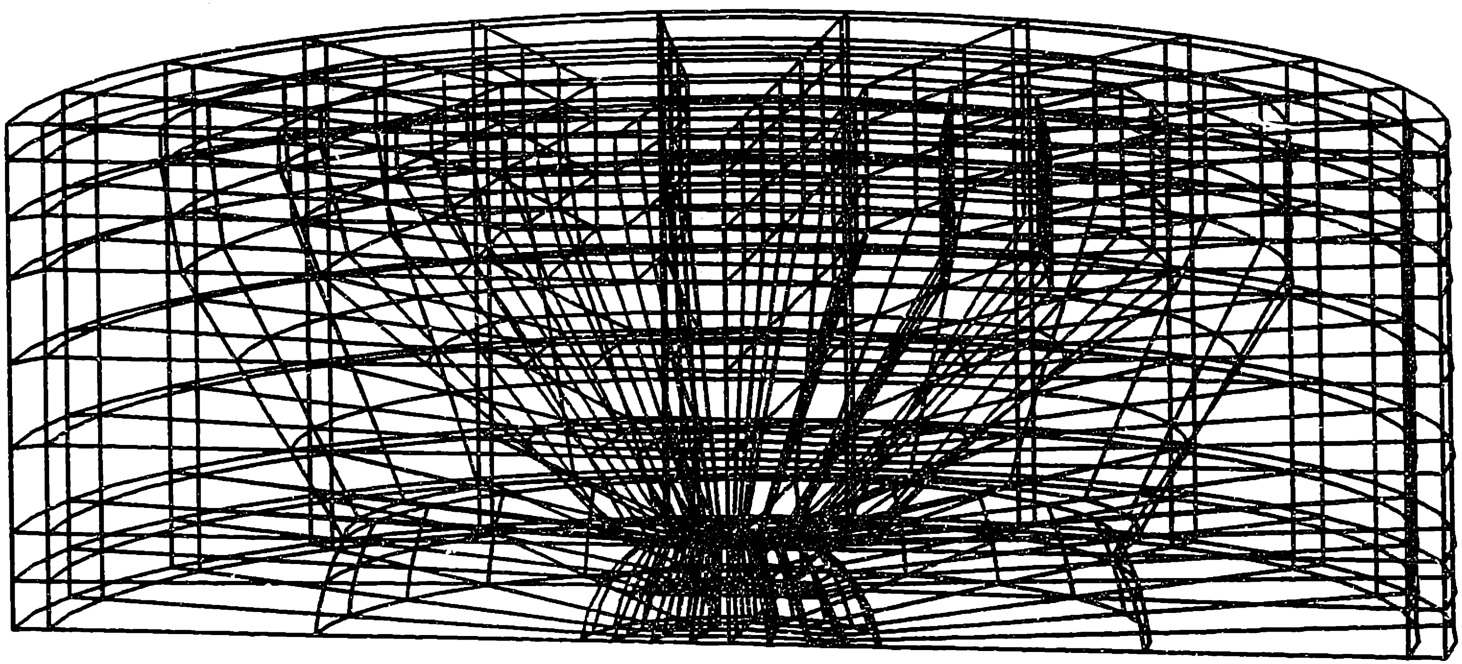

FIGURE 4: MESH OF A SP2 FEMGEN MODEL

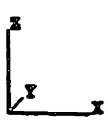

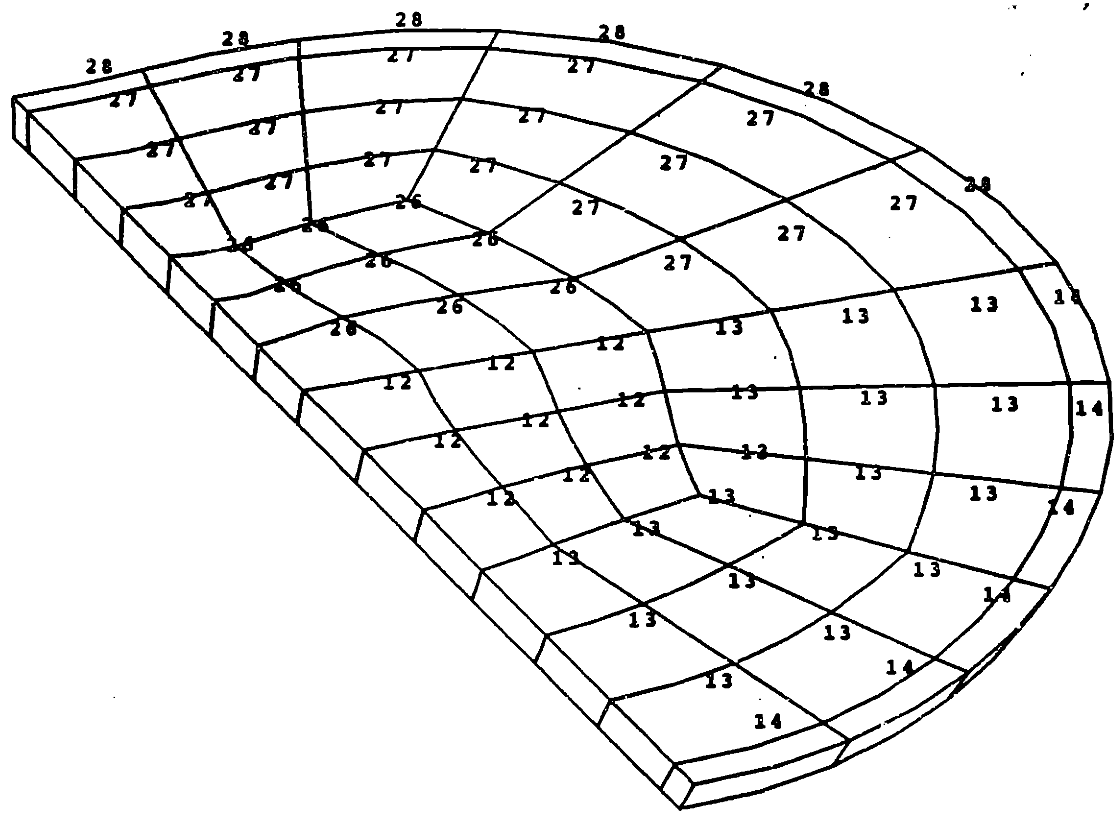

FIGURE 5 : ELEMENT GROUPS OF THE ENDPLATE

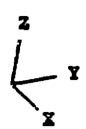

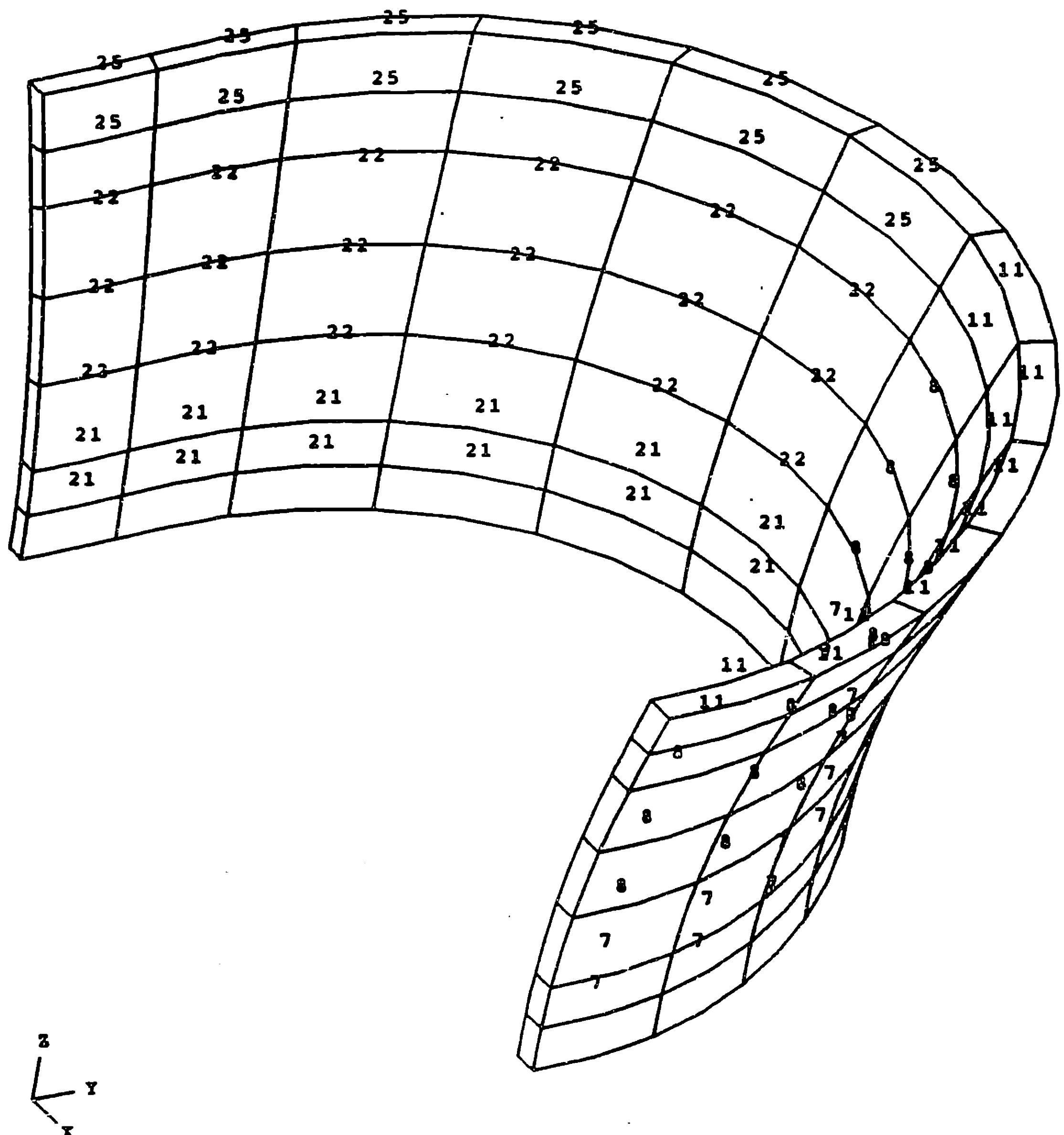

FIGURE 6: ELEMENT GROUPS OF THE CORTICAL SHELL

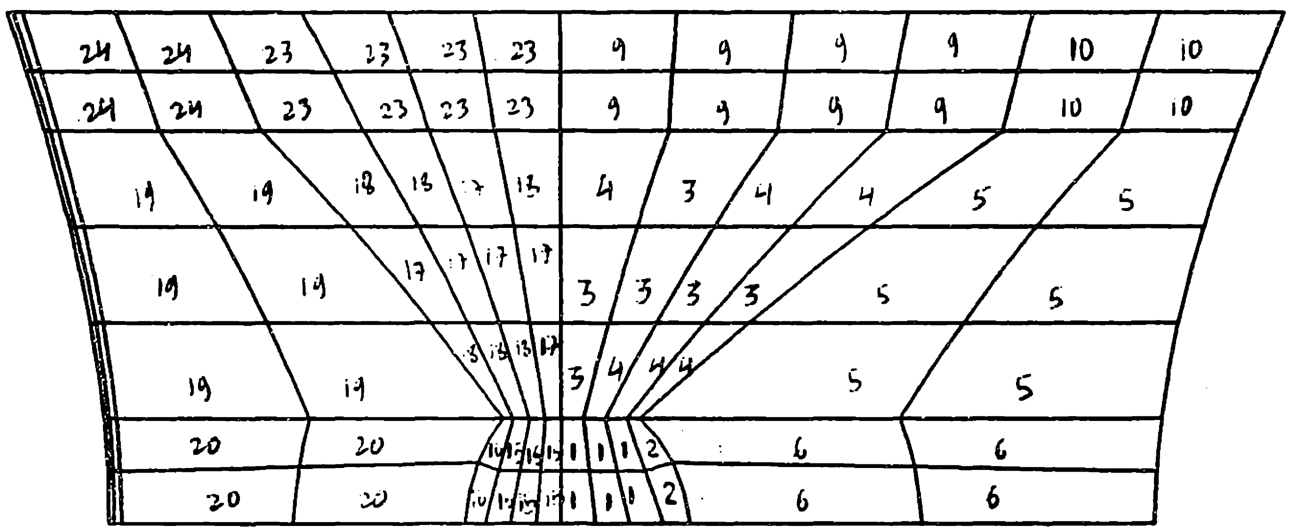

FIGURE 7 : ELEMENT GROUPS OF THE CANCELLOUS BONE

z
x

2.2.2 Endplate Biconcavity

In the models described so far (Models 3, 4, 5, 6, 7, 8 of Table 1) the endplate was modeled as a flat plate with a 1mm thickness. However, in reality the actual geometry of the endplate is a biconcave one. A program CHANGE3 was written in FORTRAN that improved the geometry. The endplate thickness is greater at the peripheral positions than at the central ones. The ratio of minimum to maximum thickness was taken as 0.87. [1] The new model took into account all of these considerations and included the biconcavity of the endplate. This produced a much more realistic geometry that would determine more accurately the mechanical behavior of the vertebral body.

[Table 1, Models 9, 10, 11, 12, 13, 14, 15, 16, 17, 18, 19, 20]

2.2.3 Modeling of metastatic defects, variation in the sphere diameter

Metastatic defects significantly alter the properties of certain areas of cancellous bone. Metastatic regions are usually spherical and can vary significantly in dimensions and properties. Initially, the spherical cavity that modeled metastatic defects, was placed in the geometric center of the vertebral body.

The size of the spherical region that modeled the metastatic defect was varied. A parameter α was defined as the ratio of the diameter of the sphere over the diameter of the cancellous bone. Two different models were produced for parameter values of 0.21 and 0.40.

[Table 1, Models 21, 22, 23, 24]

2.2.4 Variation of metastatic sphere location

The location of the cavity was also varied. Two different models were produced in which the location of the sphere had been moved radially outwards. The ratio of the distance from the center of the sphere to the geometric center of the vertebral body over the radius of the cancellous bone was defined as the parameter β The parameter values for the two models were 0.25 and 0.4 respectively.

[Table 1, Models 27,28]

2.2.5 The case of a "prismatic" defect that penetrates anterior cortex

Both cortical and cancellous bone can be affected by metastatic defects. In particular, there is the possibility that a defect could penetrate the anterior cortex, influencing the properties of both cortical and cancellous bone. A model was created in order to represent this case. The prismatic cavity was positioned at the anterior middle part of the vertebral body.(See figure 8 for location of the metastatic defect)

[Table 1, Models 29, 30]

2.3 Material properties

2.3.1 Homogeneous cancellous and cortical bone

The material properties in the basic model were for the cortical bone E=5030 N/mm^2 and for the cancellous bone E = 16.5 N/mm^2, poisson's ratio was taken as 0.2 for both cortical and cancellous bone. [13] [9] [10] The material was considered an isotropic standard engineering material.

[Table 1, Models 3, 4]

2.3.2 Variation in the material properties of the cancellous bone

Cancellous bone density is not necessarily uniform throughout the bone. Regional density values were recently obtained from the Department of Diagnostic Radiology, Henry Ford Hospital, Detroit (personal communication) that led to an improved finite element model. Specifically, the correlation of the densities for the various parts of the cancellous

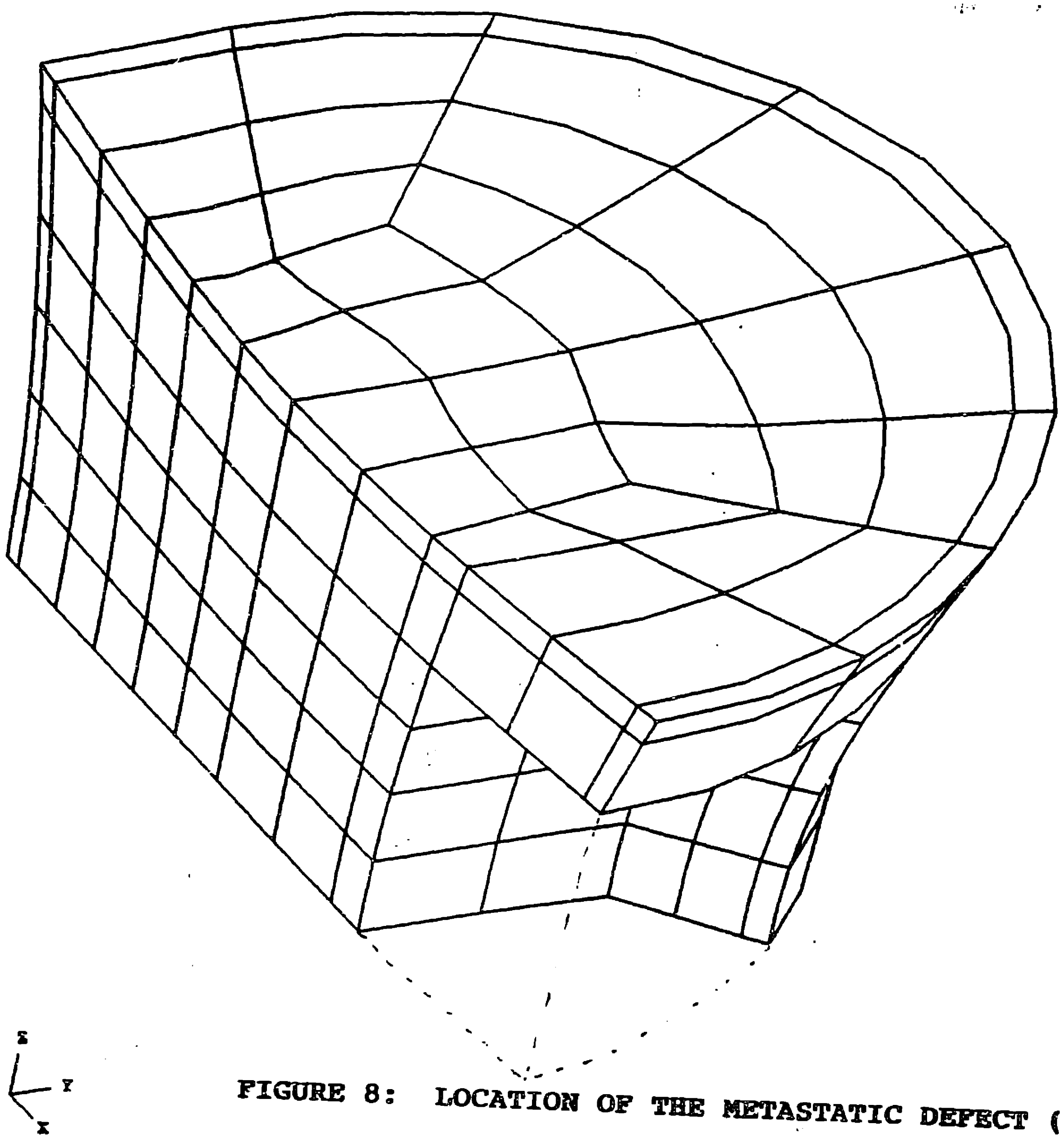

FIGURE 8: LOCATION OF THE METASTATIC DEFECT (MODELS 31-32)

bone were converted to regional values for the Young's modulus by raising the density value to the 1.2 power [11] [12]. The models produced had twelve regions of different mechanical properties for the cancellous bone as compared to one of the basic model. Figure 9 shows the twelve regions for which distinct mechanical properties were assigned.

[Table 1, Models 5, 6, 7, 8, 9, 10, 11, 12, 13, 14]

2.3.3 Strengthening of the cortical bone in the middle portion of the posterior wall

Like cancellous bone, cortical bone density is not uniform throughout the cortical shell. In particular, the middle portion of the posterior wall is stronger than the rest of the shell. An improved model that considered the variation of properties within the cortical shell was produced. The strengthening effect of the posterior wall was modeled as an increase by 20% in Young's modulus. The Young's modulus for this part of the shell was taken as 6036 N/mm^2.

[Table 1, Models 7, 8, 9, 10, 11, 12, 13, 14]

2.3.4 Modeling of the effects of osteoporosis on cancellous bone

As a result of osteoporosis cancellous bone appears to be weakened. In order for osteoporosis to be represented a model was produced that included a reduction by 50% in the strength of the cancellous bone. That reduction was performed in all regions of the cancellous bone.

[Table 1, Models 11, 12, 13, 14]

2.3.5 Modeling of the effect of osteoporosis on cortical bone

Osteoporosis also affects cortical bone. In particular osteoporotic cortical bone appears to be thinner and consequently weaker. The modeling of the weakening of the cortical bone was done by reducing the Young's modulus by 25% in all regions.

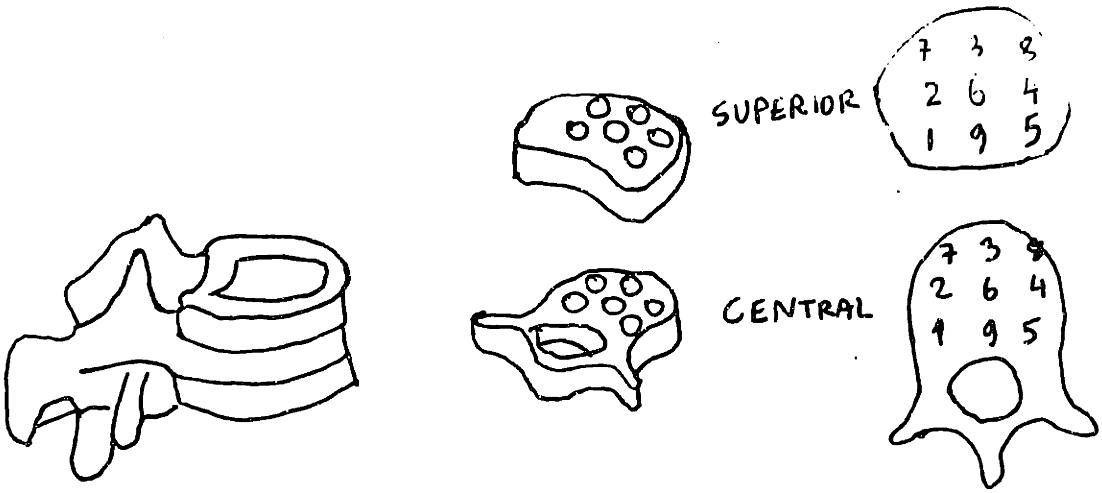

SUPERIOR (N/mm^2)	CENTRAL (N/mm^2)
E1= 17.205	E1= 17.140
E2= 16.120	E2= 16.040
E3= 16.220	E3= 16.500
E4= 16.120	E4= 16.040
E5= 17.205	E5= 17.140
E6= 16.225	E6= 16.270
E7= 16.165	E7= 16.180
E8= 16.165	E8= 16.180
E9= 16.875	E9= 17.250

FIGURE 9: REGIONAL MATERIAL PROPERTIES FOR Ecancellous

[Table 1, Models 13, 14]

2.3.6 Material properties for models with a spherical metastatic defect

Three different models were produced that differed in the Young's modulus value that was assigned to the cavity. The three different values were $10N/mm^2$, $5N/mm^2$ and $0.1N/mm^2$. The last value was assigned to the model that represented the case of having total loss of the cancellous bone as a metastatic effect.

[Table 1, Models 15, 18, 16, 19, 17, 20]

2.4 Loading conditions

2.4.1 Uniformly distributed loading on the whole of the top surface

The models that were assumed to be in uniaxial compression uniformly distributed along the endplate surface were subjected to a pressure of $1.24N/mm^2$, corresponding to a weight loading of 868 N associated with loading present in normal activities, such as lifting and changes in position [13].

[Table 1, Models 3, 5, 7, 9, 11, 13, 15, 16, 17, 21, 23, 25, 27]

2.4.2 Peripherally Distributed loading

The models that were assumed to be under peripherally loading conditions were subjected to a pressure of $1.96N/mm^2$ along the three outer layers of elements of the endplate surface(See figure 10).

[Table 1, Models 4, 6, 8, 10, 12, 14, 18, 19, 20, 22, 24, 26, 28]

2.4.3 Uniformly Distributed Loading corresponding to bending forward by 20°

The higher than normal pressure of 1.85 N/mm^2 was corresponding to the pressure exerted on the vertebral body at the 20° bending case [2], [3]. [Table 1, Model 29, 31]

2.4.4 Unevenly Distributed Loading, with maximum at the anterior part of the vertebral body

The pressures were unevenly distributed on the top surface at four different regions. Figure 11 shows these regions and the corresponding pressure values for each region. These values were taken from Horst et al [3].

[Table 1, Model 30, 32]

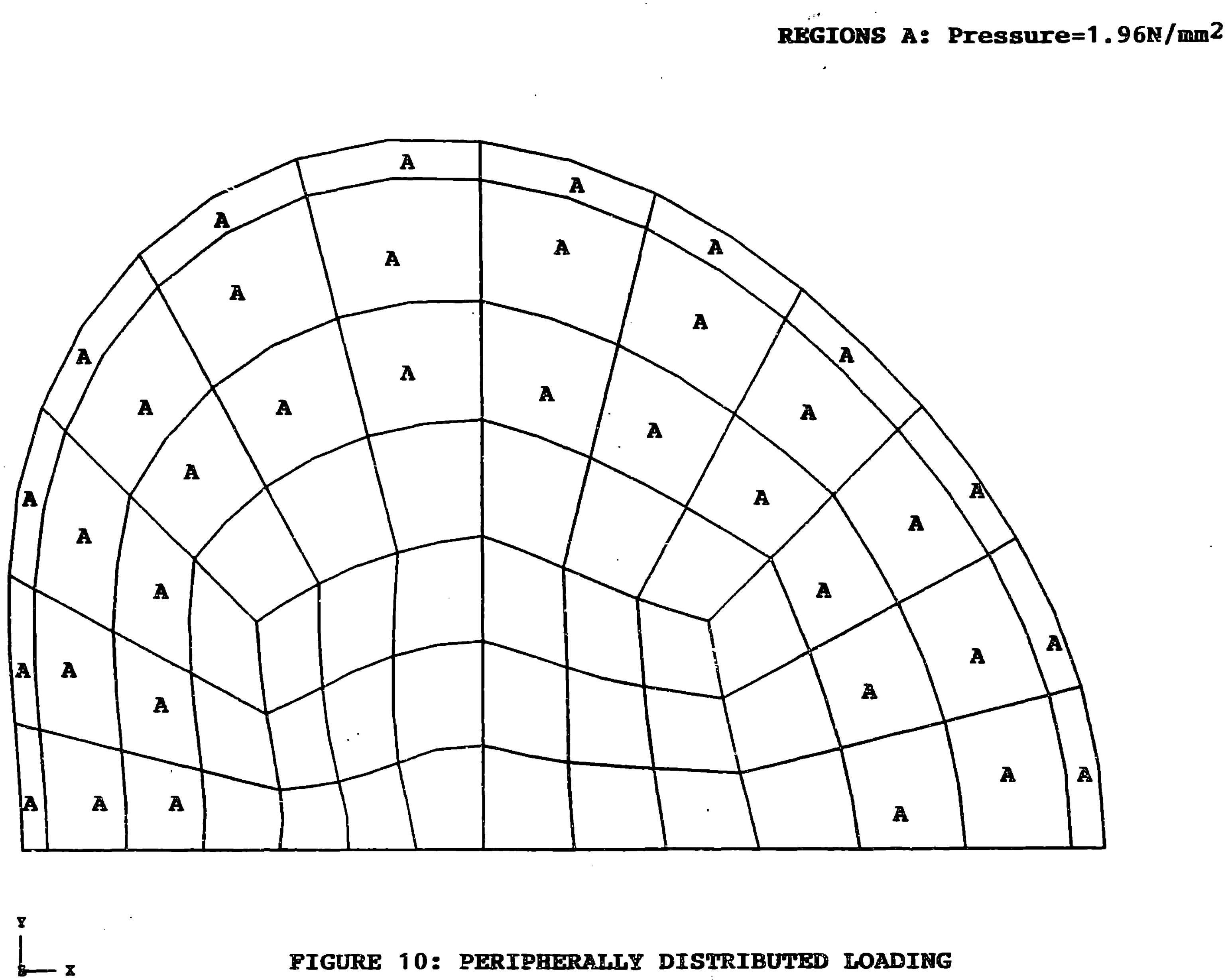

FIGURE 10: PERIPHERALLY DISTRIBUTED LOADING

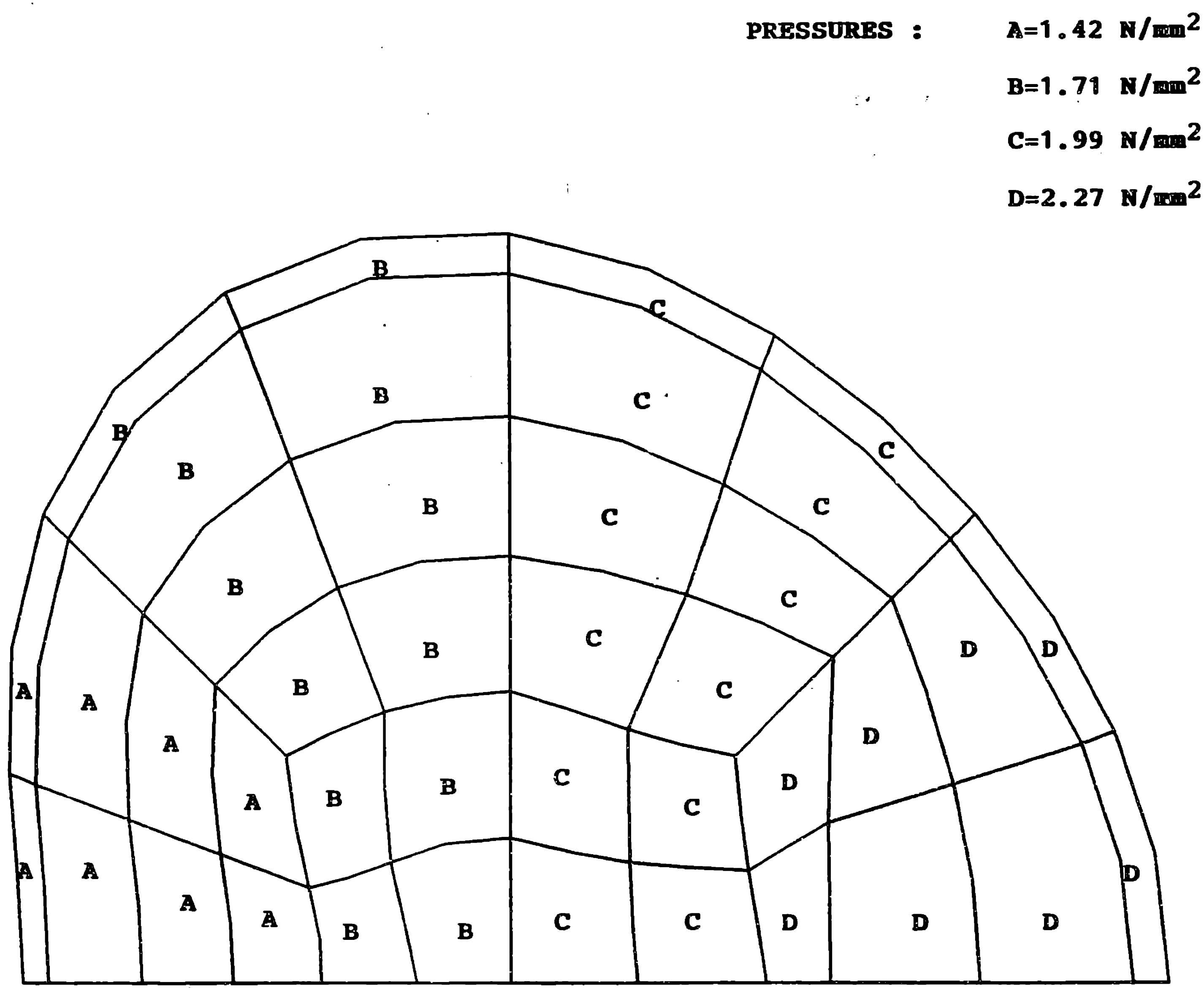

FIGURE 11: NON-UNIFORM PRESSURE DISTRIBUTION

Chapter 3

RESULTS

Using the post-processor FEMVIEW the following data were obtained:

- Displacements
- Von-Mises Stresses
- Principal Stresses

In order for quantitative comparisons to be made, certain nodes had to be isolated and examined with respect to the above data. These nodes were selected by global examination of the maximums and minimums for the above criteria.

Numerical data were collected and presented in tables. Also various plots of principal stress, Von Mises stress and displacement were collected by using the post-processor FEMVIEW.

There were nine comparison cases for which, in order for conclusions to be reached certain models were isolated and compared.

In addition to the numerical results, there were also graphs produced that qualitatively described the displacement, principal stress and Von Mises stress fields throughout the vertebral body. Figure 12 shows the displacement field for model 3. Also Figure 13 shows the principal stress field (P3) for the same model (Contour graph in 3 levels). Figure 14 shows the principal stresses in vectorial representation. Also Figure 15 shows the Von Mises stress field in 3 contours.

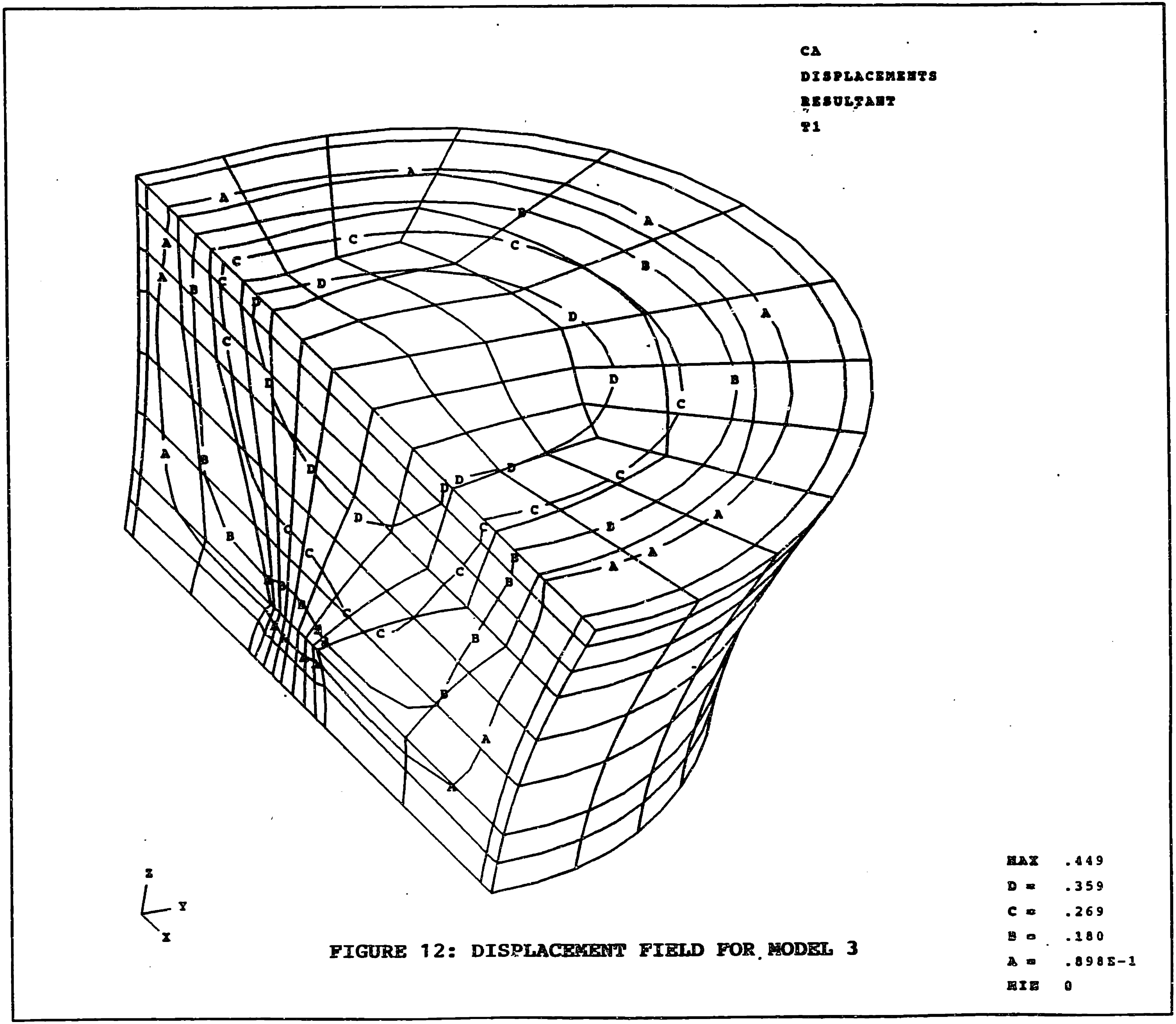

FIGURE 12: DISPLACEMENT FIELD FOR MODEL 3

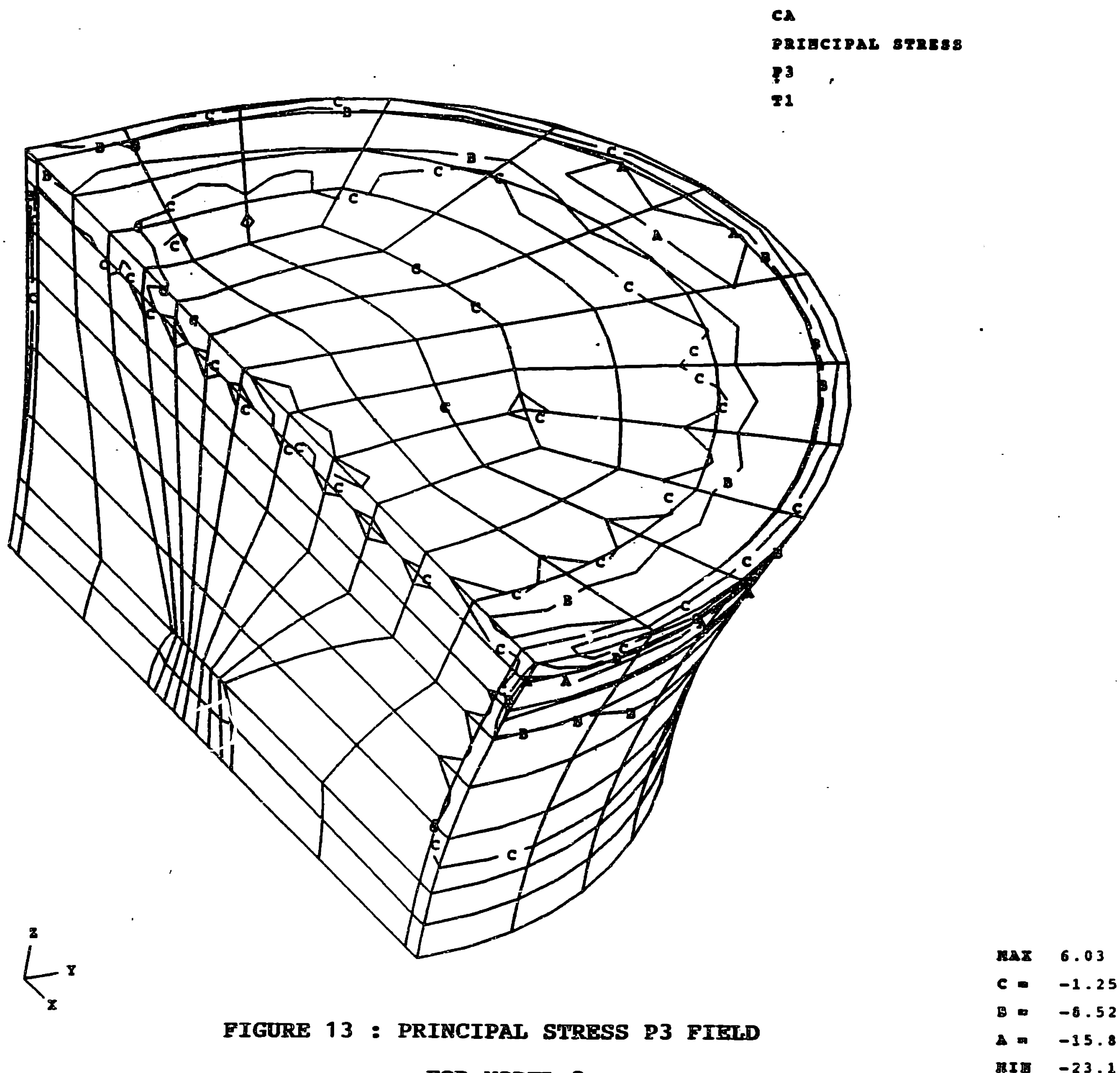

FIGURE 13 : PRINCIPAL STRESS P3 FIELD

FOR MODEL 3

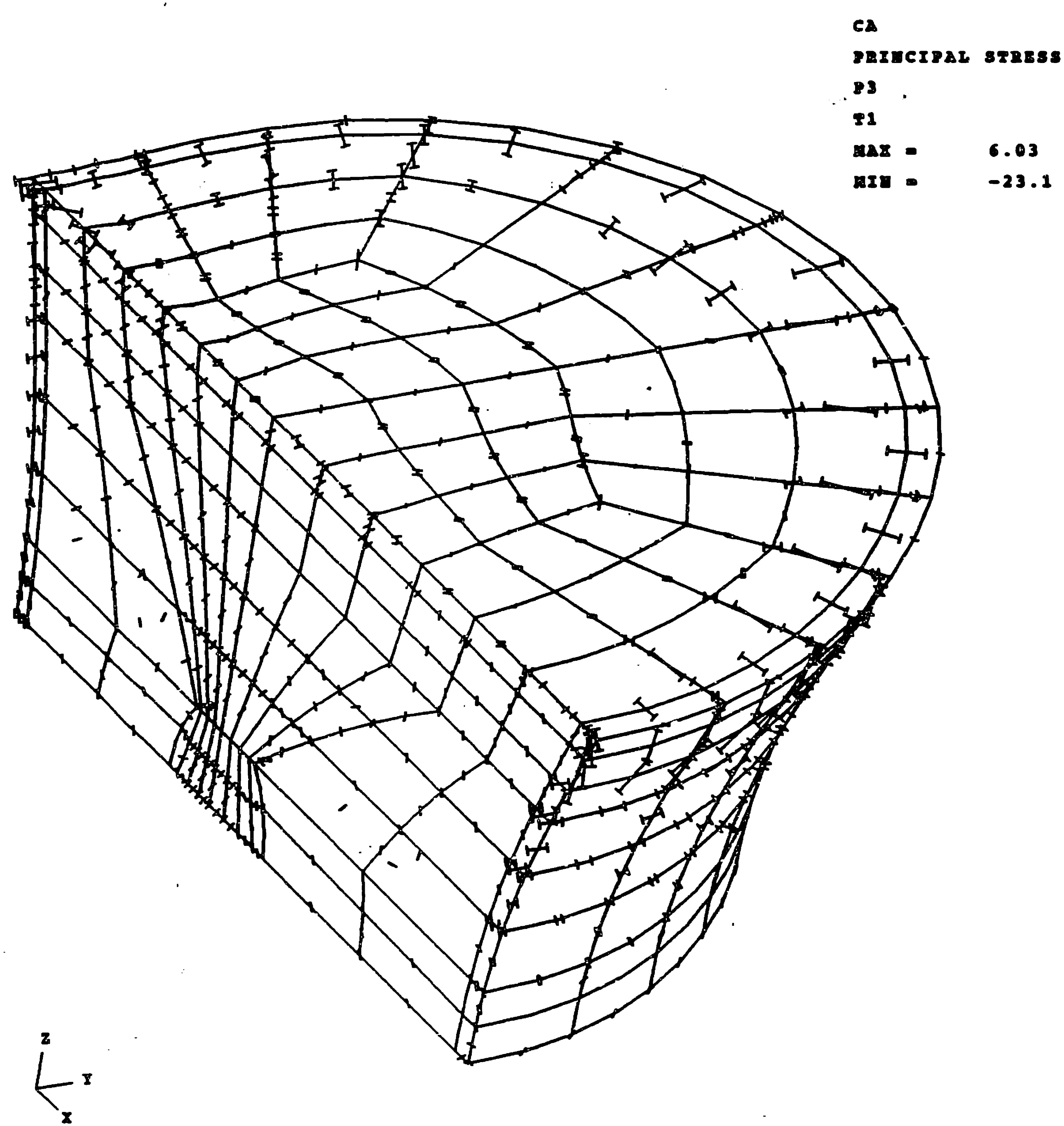

FIGURE 14: PRINCIPAL STRESS P3 (VECTORIAL REPRESENTATION)

FOR MODEL 3

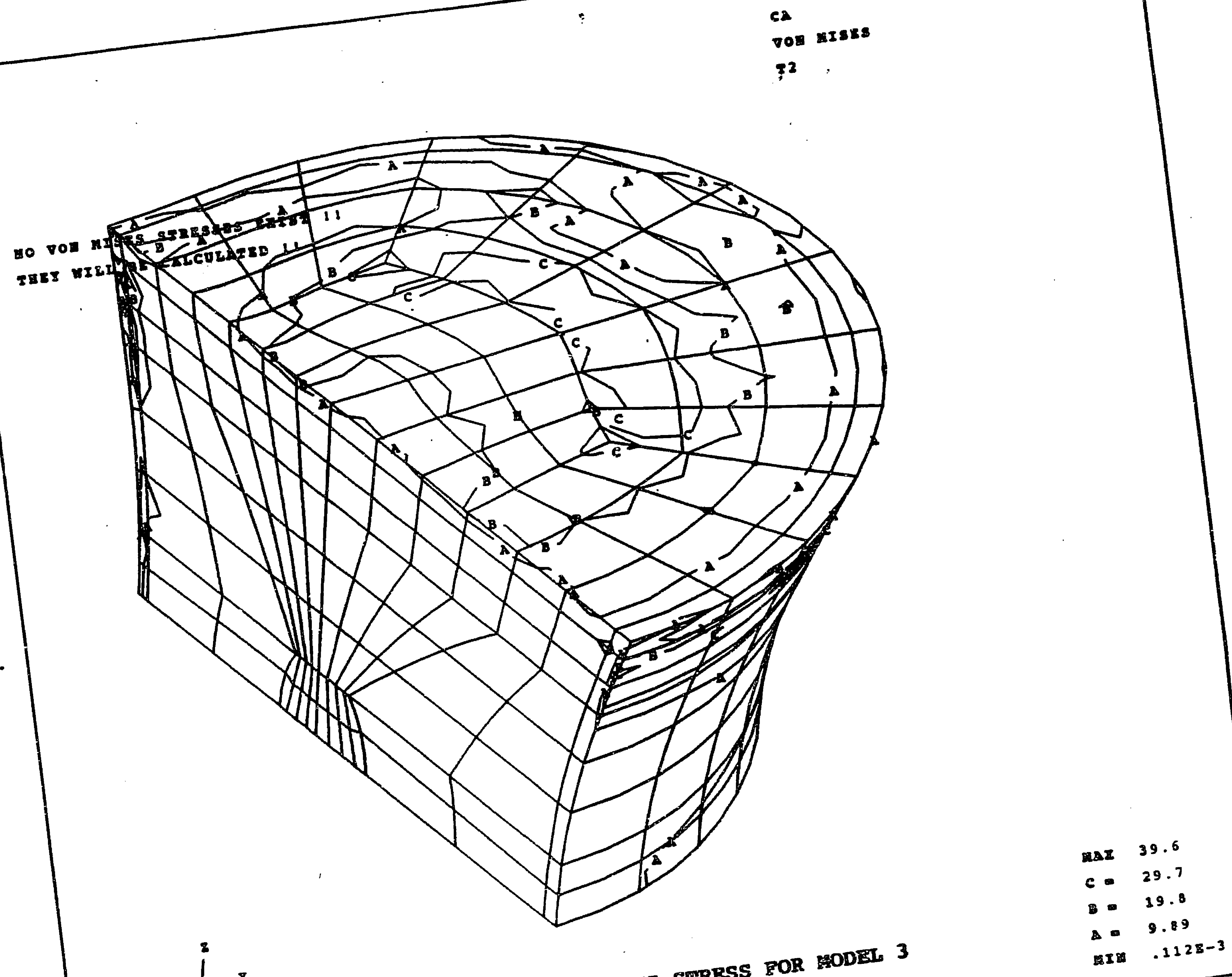

FIGURE 15: VON MISES STRESS FOR MODEL 3

3.1 NORMAL CASE

3.1.1 Examination of the effects of variable regional E cancellous

For this comparison, models 3&5 were studied for the uniformly distributed pressure case and models 4&6 for the peripherally distributed pressure case. The data obtained as well as the calculated percentage changes are presented in Table 2. Nodes 1390 and 397, where maximum displacement occured, are located at the top surface of the endplate. Peak values for principal stresses were obtained at nodes 2607 and 4 which are located at the cortical shell directly below the endplate. Finally, peak values for Von Mises were obtained at nodes 2145 & 2187 which are both located on the upper surface of the endplate.

		UNIFORMLY DISTR.PRESS			PERIPHERALLY DIS.PRES		
	Nodes	Model 3	Model 5	%	Model 4	Model 6	%
Displ. [mm]	1390	0.449	0.456	+1.6	-	-	-
	397	-	-	-	0.188	0.190	+1.1
Princ. Stress P3 [N/mm²]	2607	-23.1	-23.4	+1.3	-	-	-
	4	-	-	-	-25.2	-25.4	+0.8
at the endplate [N/mm²]	1	-19.7	-19.8	+0.5	-	-	-
	3	-	-	-	-24.8	-24.9	+0.4
Von Mises Stress [N/mm²]	2145	39.6	39.9	+0.8	-	-	-
	2187	-	-	-	51.7	51.8	+0.2

TABLE 2: EFFECTS OF VARIABLE Ecancellous

3.1.2 Examination of the effect of the increase in E cortical in the posterior wall

Models 5&7 were examined for the uniformly distributed pressure case and models 6&8 for the peripherally distributed pressure one. The data are presented in Table 3. Nodes 1390 and 397, where maximum displacement occured, are located at the top surface of the endplate. Peak values for principal stresses were obtained at nodes 2607 and 4 which are located at the cortical shell directly below the endplate. Finally, peak values for Von Mises were obtained at nodes 2145 & 2187 which are both located on the upper surface of the endplate.

		UNIFORMLY DISTR.PRESS			PERIPHERALLY DIS.PRES		
	Nodes	Model 5	Model 7	%	Model 6	Model 8	%
Displ. [mm]	1390	0.456	0.456	+0.00	-	-	-
	397	-	-	-	0.190	0.190	+0.00
Princ. Stress P3 [N/mm^2]	2607	-23.4	-23.4	+0.00	-	-	-
	4	-	-	-	-25.4	-25.4	+0.00
at the endplate [N/mm^2]	1	-19.8	-19.8	+0.00	-	-	-
	3	-	-	-	-24.9	-24.9	+0.00
Von Mises Stress [N/mm^2]	2145	39.9	39.9	+0.00	-	-	-
	2187	-	-	-	51.8	51.8	+0.00

TABLE 3:EFFECT OF STRENGTHENING MIDDLE POSTERIOR WALL

3.1.3 Effect of Biconcavity

Models 7&9 were examined for the uniformly distributed pressure case and models 8&10 for the peripherally distributed pressure one. Nodes 1390, 397 and 396, where maximum displacement occured, are located at the top surface of the endplate. Peak values for principal stresses were obtained at nodes 2607, 4 and 5 which are located at the cortical shell directly below the endplate. Finally, peak values for Von Mises were obtained at nodes 2145, 2187 and 646 which are all located on the upper surface of the endplate. This data are presented in Table 4

		UNIFORMLY DISTR.PRESS			PERIPHERALLY DIS.PRES		
	Nodes	Model 7	Model 9	%	Model 8	Model10	%
Displ.	1390	0.456	0.420	-7.9	-	-	-
[mm]	397	-	-	-	0.190	0.202	+6.3
	396					0.203	
Princ.	2607	-23.4	-18.5	-20.9	-	-	-
Stress	4	-	-	-	-25.4	-24.2	-4.7
P3	5	-	-21.1	-	-	-	-
[N/mm^2]							
at the	1	-19.8	-8.9	-54.7	-	-	-
endplate	3	-	-16.4	-	-24.9	-23.0	-7.6
[N/mm^2]							
Von	2145	39.9	33.9	-15.1	-	-	-
Mises	2187	-	-	-	51.8	52.2	+0.8
Stress	646	-	34.4	-	-	-	-
[N/mm^2]							

TABLE 4: EFFECT OF BICONCAVITY

3.2 OSTEOPOROTIC BONE

3.2.1 Pathology, effect of reduction in E cancellous by 50%

Models 9&11 were examined for the uniformly distributed pressure case and models 10&12 for the peripherally distributed pressure one.

Nodes 1390, 396, 397 and 1151 where maximum displacement occured, are located at the top surface of the endplate. Peak values for principal stresses were obtained at nodes 2607, 4, 5 and 431 which are located at the cortical shell directly below the endplate. Finally, peak values for Von Mises were obtained at nodes 2145, 2187, 646 and 2680 which are all located on the upper surface of the endplate.

The data are presented in Table 5.

		UNIFORMLY DISTR.PRESS			PERIPHERALLY DIS.PRES		
	Nodes	Model 9	Model 11	%	Model 10	Model 12	%
Displ.	1390	0.420	0.704	+67.6	-	-	-
[mm]	397	-	-	-	0.202	0.314	+55.5
	396			-	0.203	0.313	+54.2
	1151	-	0.708	-	-	-	-
Princ.	2607	-18.5	-	-	-	-	-
Stress	4	-	-	-	-24.2	-	-
P3	5	-21.1	-31.1	+47.4	-	-31.0	-
[N/mm^2]	431	-	-32.5	-	-	-	-
at the	1	-8.97	-	-	-	-	-
endplate	3	-16.4	-20.5	+25.0	-23.0	-26.4	+14.8
[N/mm^2]	1284	-	-25.6	-	-	-	-
Von	2145	33.9	-	-	-	-	-
Mises	2187	-	-	-	52.2	57.0	+9.20
Stress	646	34.4	43.3	+25.9	-	-	-
[N/mm^2]	2680	-	57.1	-	-	-	-

TABLE 5: EFFECT OF REDUCTION IN Ecancellous

3.2.2 Pathology, effect of reduction in E cortical by 25%

Models 11&13 were examined for the uniformly distributed pressure case and models 12&14 for the peripherally distributed pressure one.

Nodes 1390, 397, 396 and 1151 wheιє maximum displacement occured, are located at the top surface of the endplate. Peak values for principal stresses were obtained at nodes 431 and 5 which are located at the cortical shell directly below the endplate. Finally, peak values for Von Mises were obtained at nodes 2680, 2187 and 646 which are all located on the endplate.

The data are presented in Table 6.

		UNIFORMLY DISTR.PRESS			PERIPHERALLY DIS.PRES		
	Nodes	Model 11	Model 13	%	Model 12	Model 14	%
Displ.	1390	0.704	-	-	-	-	-
[mm]	397	-	-	-	0.314	0.353	+12.4
	396				0.313		
	1151	0.708	0.768	+8.47	-	-	-
Princ.	5	-31.1			-31.0	-28.0	+9.68
Stress	431	-32.5	-27.3	-16.0	-	-	-
P3 [N/mm^2]							
at the endplate [N/mm^2]	3	-	-18.7	-	-26.4	-25.0	-5.3
Von	2187	-	-	-	57.0	55.1	-3.33
Mises	646	43.3	-	-	-	-	-
Stress [N/mm^2]	2680	57.1	45.4	-20.5	-	-	-

TABLE 6: EFFECT OF REDUCTION IN Ecortical

3.3 METASTATIC DEFECTS

3.3.1 Pathology, effect of the spherical metastatic defect

Models 9, 15, 16, 17 were examined for the uniformly distributed pressure case and models 10, 18, 20 for the peripherally distributed pressure one. The data are presented in Table 7 and 8. Three graphs were also produced that plotted displacement, principal stress P3 and Von Mises stress versus E cancellous for the spherical cavity. These graphs appear in Figures 16, 17, 18.

UNIFORMLY DISTRIBUTED PRESSURE

	Nodes	Model 9	Model 15	Model 16	Model 17
Displ.	1390	0.420			
[mm]	1136		0.174	0.221	0.320
	1154		0.425	0.433	0.448
Princ.	2607	-18.5	-	-	-
Stress	5	-	-21.2	-21.3	-21.5
P3					
[N/mm^2]					
at the	1130	-	-6.7	-5.1	-0.7
endplate	3	-16.4	-	-	-
[N/mm^2]					
Von	2145	33.9	-	-	-
Mises	1130	-	6.5	5.1	3.9
Stress	646	-	34.4	34.3	34.3
[N/mm^2]					

TABLE 7: VARIATION IN Esphere (UNIFORM LOADCASE)

GRAPH1 13-MAY-90 18:24 Page 1

Figure 16: Max. Displacement vs. E metastatic sphere

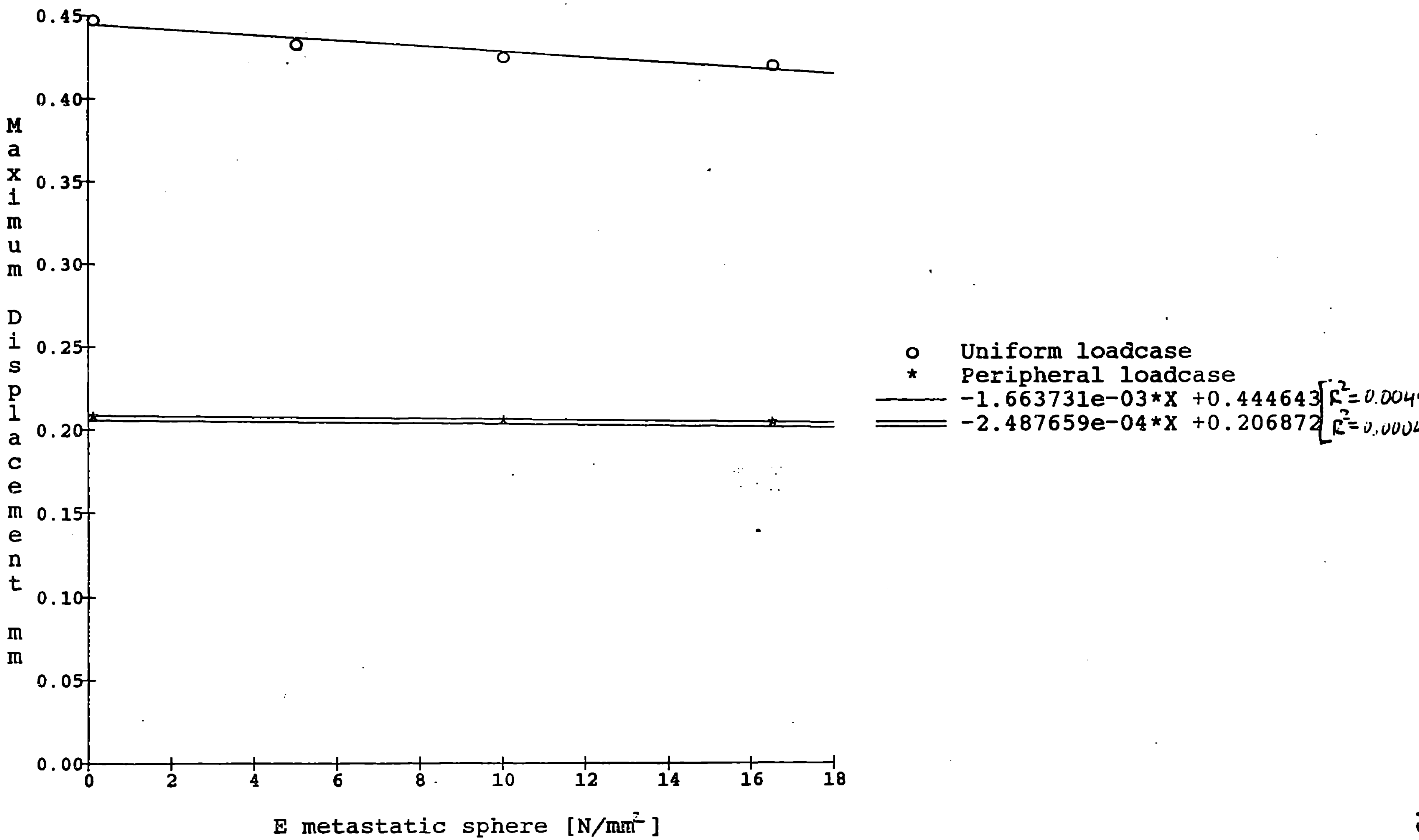

Figure 17: Max. Absolute Principal Stress P3 vs. E metastatic sphere

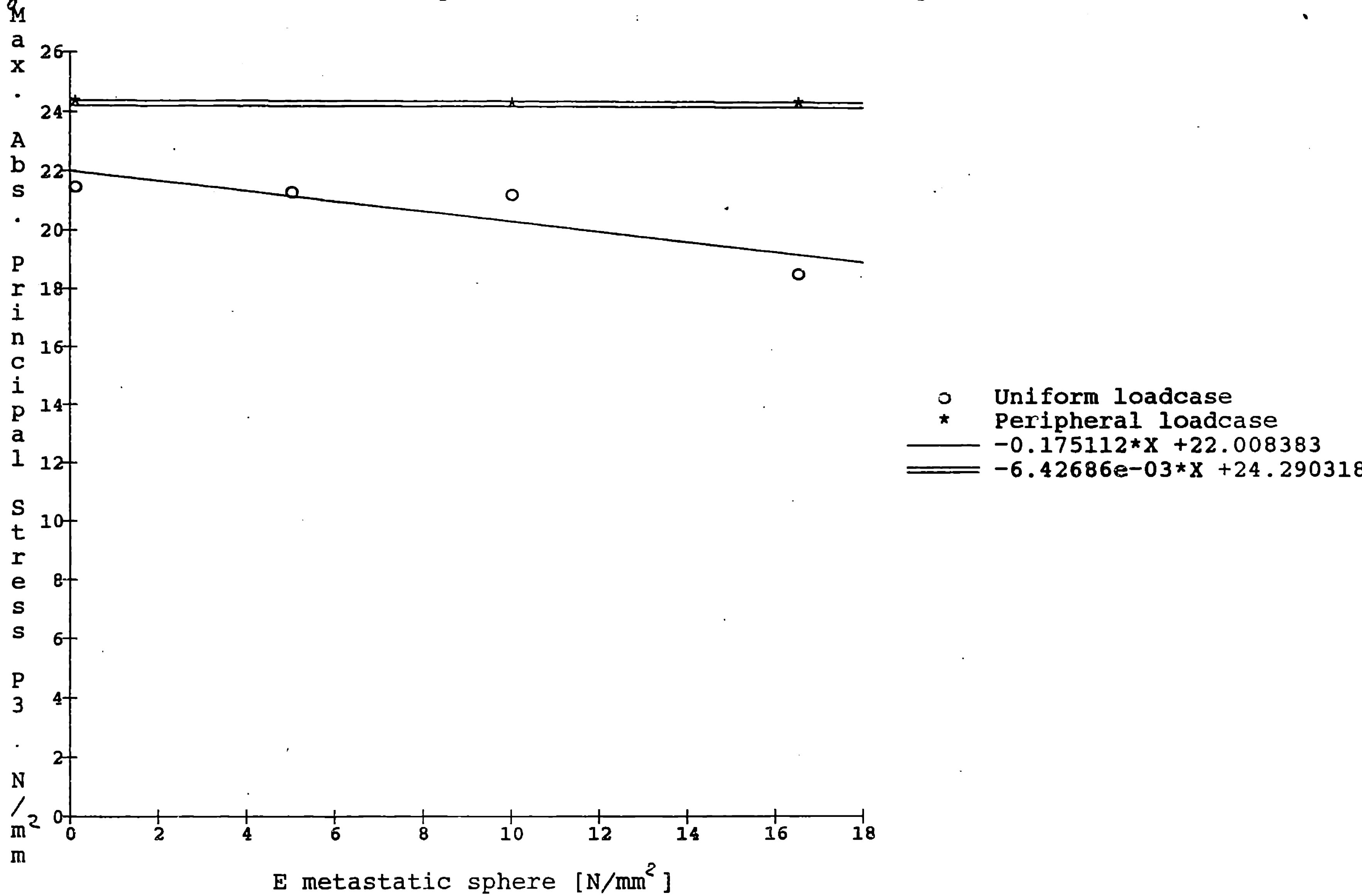

$R^2 = 0.878$

$R^2 = 0.032$

Figure 18: Max. VonMises vs. E metastatic sphere

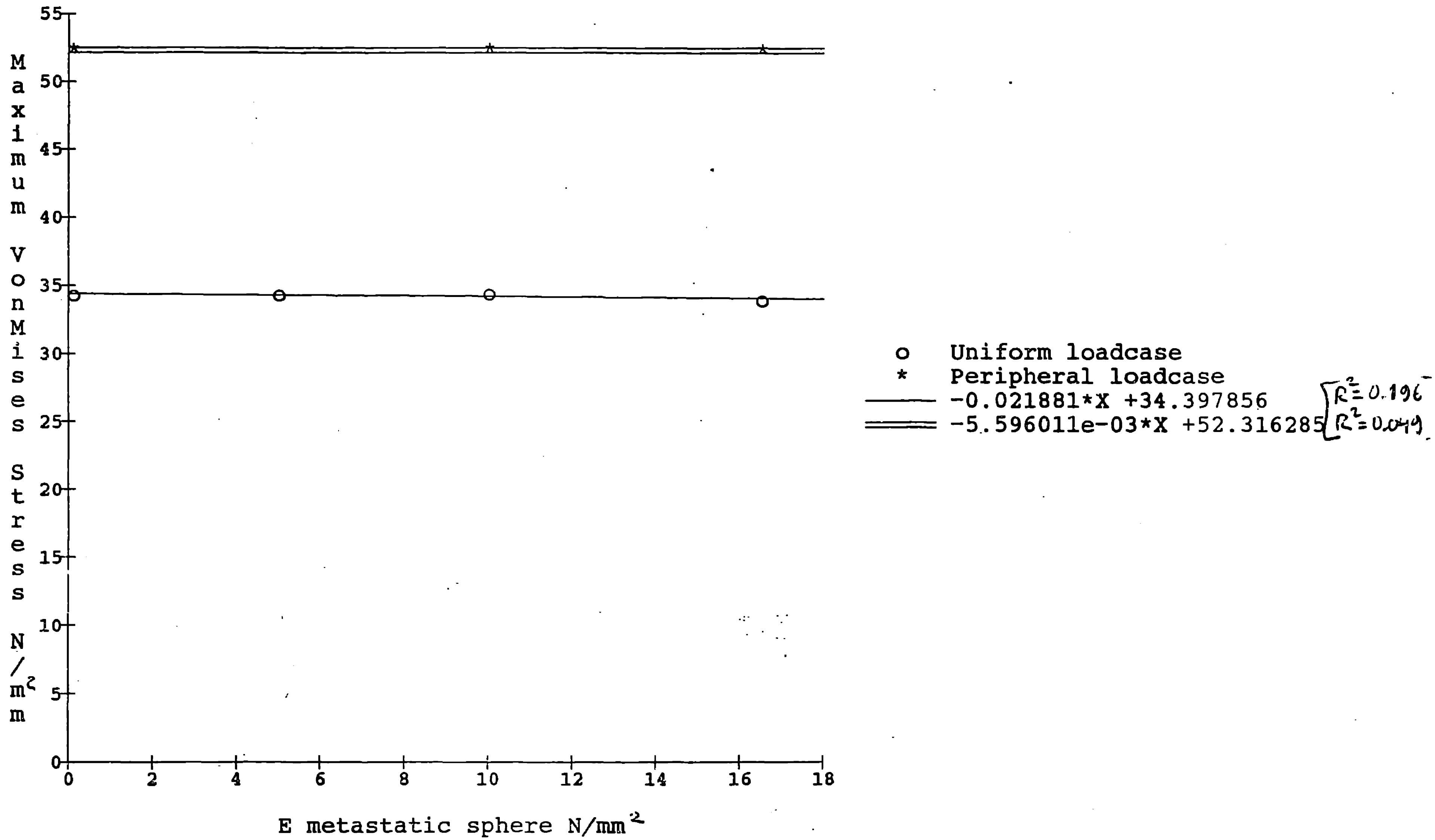

PERIPHERALLY DISTRIBUTED PRESSURE

	Nodes	Model 10	Model 18	Model 20
Displ. [mm]	396	0.203	0.204	0.207
Princ. Stress P3 [N/mm^2]	4	-24.2	-24.2	-24.3
Von Mises Stress [N/mm^2]	2187	52.2	52.3	52.3

TABLE 8: VARIATION IN Esphere (PERIPHERAL LOADCASE)

3.3.2 Effect of variation in the metastatic sphere diameter

Models 21&9 were examined for the uniformly distributed pressure case and models 22&10 for the peripherally distributed pressure case. The data are presented in Table 9.

		UNIFORMLY DISTR.PRESS		PERIPHERALLY DIS.PRES	
	Nodes	Model 9	Model 21	Model 10	Model 22
Displ.	1390	0.42	-	-	-
[mm]	396	-	-	0.20	-
	848	-	2.2	-	-
% change			+433 %		
Princ.	2607	-18.5	-	-	-
Stress	4	-	-	-24.2	-
P3	2433	-	-74.1	-	-
[N/mm^2]					
% change			+301 %		
Von	2187	-	-	52.2	-
Mises	646	34.4			
Stress	184	-	184.0	-	
[N/mm^2]					
% change			+435 %		

TABLE 9: VARIATION OF PARAMETER a

3.3.3 Effect of the metastatic sphere location

Models 9, 25 and 27 were examined for the uniformly distributed pressure case. The data are presented in Table 10. Figure 19 shows the variation of maximum principal stresses with the parameter β.

		UNIFORMLY DISTRIBUTED PRESSURE		
		Model 9	Model 25	Model 27
	Nodes	b=0.0	b=0.21	b=0.4
Disp.	1390	0.42	-	-
[mm]	880	-	0.40	-
	1936	-	-	0.46
% change			-5 %	+11 %
Princ.	5	-21.1	-	-
Stress	13	-	-39.9	-
P3	2627	-	-	-23.3
[N/mm^2]				
% change			+89 %	+10 %
Von	646	34.4	-	-
Mises	207	-	79.0	-
Stress	2690	-	-	55.9
[N/mm^2]				
% change			+129 %	+62 %

TABLE 10: VARIATION OF PARAMETER b

3.3.4 Effect of the prismatic defect

Models 29&31 were examined for the uniformly distributed pressure case and models 30&32 for the uneven distributed pressure case. The data are presented in Table 11.

	Nodes	UNIF. DISTR.PRESS. Mod 29	Mod 31	UNEVEN DISTR.PRESS Mod 30	Mod 32
Disp.	398	1.1	1.4	1.2	1.5
[mm]	257	-	1.7	-	1.9
% change			+50 %		+83 %
Princ.	21	-21.3		-26.2	
Stress	23		-33.7		-40.8
P3					
[N/mm^2]					
% change			+58 %		+91 %
Von	634	32.5		32.5	
Mises	132		44.43		58.3
Stress					
[N/mm^2]					
% change			+36 %		+79 %

TABLE 11: PRISMATIC DEFECT CASE vs. NORNAL CASE

Figure 19: Maximum Absolute Principal Stress P3 vs. parameter b

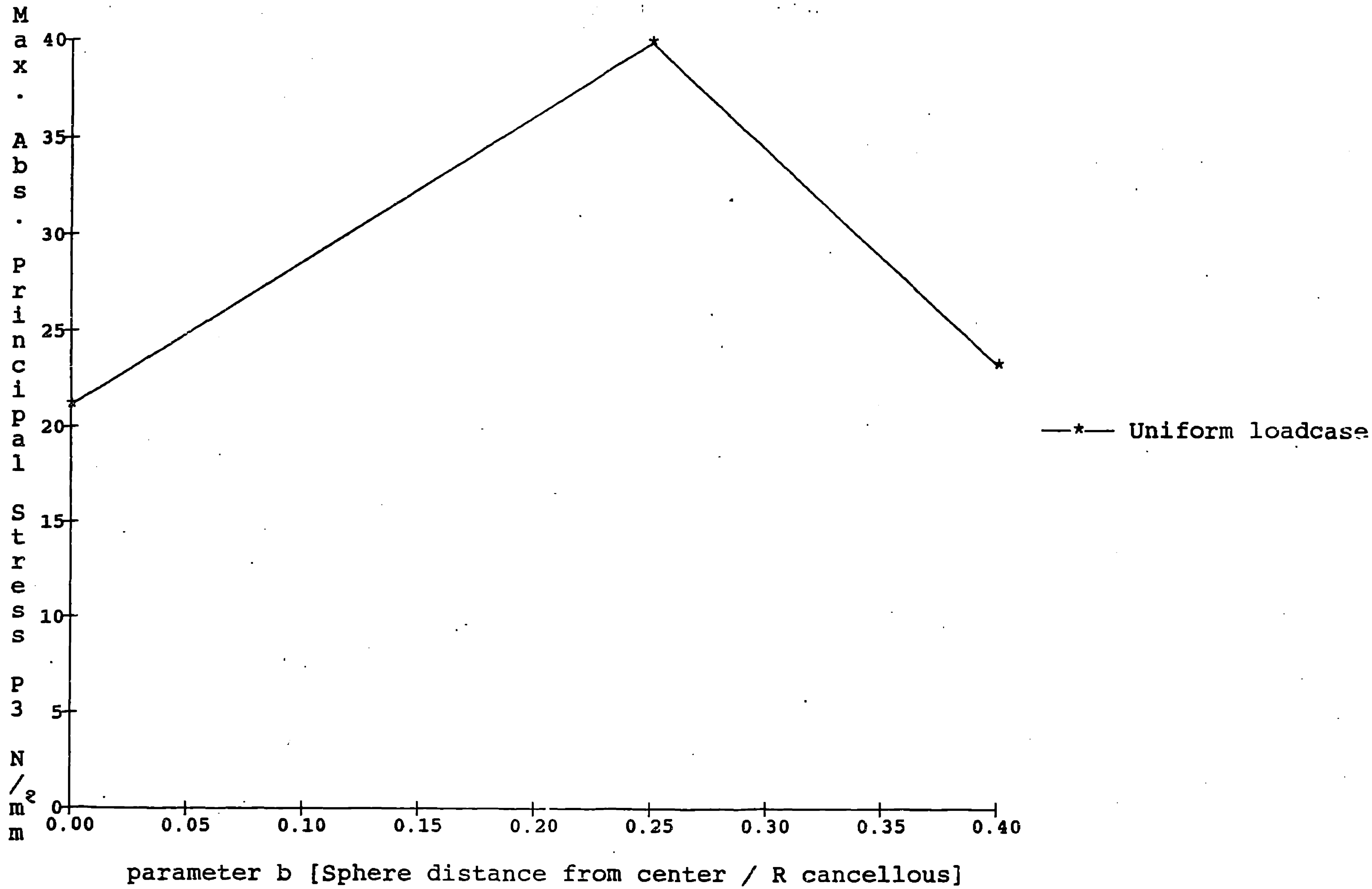

Chapter 4

DISCUSSION

4.1 NORMAL CASE

In interpreting the results, three criteria were utilized, nodal displacement, principal stress in the P3 direction and Von Mises effective stress. Von Mises stress was determined to be the most useful of the criteria, mainly because it represents the stress condition of a point in the vertebral body by taking into account all normal and shear stresses but presenting them in a scalar rather than a tensorial form.

The utilization of variable cancellous bone density depending on the region did not have a strong effect in the displacements and stresses generated. There was a 1-2% increase in maximum displacement and a 0.2-1.3% increase in maximum stresses. Consequently, the simplified model with constant E cancellous proved to accurately describe the mechanical behavior of the vertebral body.(See Table 2) In this study the models that were utilized for the strength analysis of the vertebral body for the pathological case of metastatic defects did not include variable E cancellous since the simplified model was proved to be sufficient.

The increase in E cortical in the posterior wall had a very insignificant effect on the displacements and stresses throughout the vertebral body. There was a slight increase in the associated stresses in the middle posterior wall (as well as a decrease in displacements) but the maximum stresses were much higher than the ones in the middle posterior wall and remained unchanged. Therefore, the effects were located only within the middle posterior wall and were accompanied by a decrease in regional stresses in the cancellous bone elements which were attached to the middle posterior cortical wall. (See Table 3)

The improvement in the geometric description of the vertebral body that included biconcavity of the endplate, had different effects depending on the loading case. In the uniformly distributed case maximum displacement was lower, principal stresses were much lower and Von Mises stresses were also reduced but to a lower extent. In the peripherally distributed case the peak displacements appeared to be higher, the principal stresses were lower and the Von Mises stresses were affected by very little. The displacement changes ranged from -8% to +6%, while the principal stress changes from -5% to -55%. The Von Mises stress changes ranged from 1% to 52%. Hence, it is concluded that the incorporation of biconcavity into the geometry of the model significantly influenced the stresses and displacements and was therefore necessary in order to accurately model the mechanical behavior of the vertebral body. It was therefore included in all of the subsequently produced models. (See Table 4)

4.2 PATHOLOGICAL CASE: OSTEOPOROSIS

In the pathological case in which due to osteoporosis we have a reduction in mechanical properties by 50% the effects were dramatic. The effects were most noticeable in the uniformly distributed case for which there was a 67.6% increase in maximum displacement, a 47.4% increase in maximum stress and a 25.9% increase in Von Mises stresses. Also in the peripherally distributed case the effects were strong but due to the reason that the pressure load is mainly sustained by the outer layers of elements, the resulting percentage changes were not as dramatic as in the uniformly distributed case. (See Table 5)

Examining the effect of osteoporosis on cortical bone, mainly what was modeled as a reduction in mechanical properties by 25% it was concluded that it has serious consequences in the resulting displacements and stresses. As anticipated, the displacement increases were larger for the peripherally distributed pressure case. Also the stresses were lower at the cortical shell but significantly higher at the cancellous bone regions. The maximum value for principal stresses was decreased by 16 % for the uniform loading case and increased by 10 % in the peripheral loading case. The corresponding maximum displacements were increased by 9 and 12 % for the respective loading cases.(See Table 6)

4.3 PATHOLOGICAL CASE : METASTATIC DEFECTS

By examining Figures 17 it can be concluded that the maximum principal stress increases with decreasing E sphere and also that this increase is is minimized as the E values approach zero. Von Mises stresses are relatively constant with variable E sphere for both loading conditions. Also, the maximum displacement is kept relatively unchanged with decreasing E sphere for both loading conditions as well. Hence, the effect of a metastatic effect in the geometric center of the vertebral body is not major, as long as its dimensions are small.

The effects of increasing the metastatic sphere diameter were of major importance to the mechanical behavior of the vertebral body. The parameter α was varied from 0.21 to 0.40. The almost doubling of the sphere diameter gave rise to as much as 433% to the peak displacement and of 300% to principal stresses as well as 435 % to Von Mises stresses. Therefore, the size of the spherical cavity was the most important factor in influencing the strength of the vertebral body.

The change in location of the metastatic sphere showed no specific trend in terms of correlating the parameter β with the observed change in displacements and stresses. Specifically, maximum displacement decreased as the sphere moved radially outwards but increased as it further approached the cortical shell. Maximum principal stresses increased by as much as 89% for β=0.25 but then were reduced to only 10% of the original value for β=0.40. Maximum Von Mises stresses also exhibited similar behavior by reaching 130% of the original value for β=0.25 and dropping to 63% for β=0.4. The increase in the observed stresses can be qualitatively attributed to the non-symmetrical geometry that gives rise to the stresses in the cortical shell closer to the defect. However, the effect should have been amplified for β=0.4, instead it showed a significant decrease.

The prismatic defect that penetrated the anterior cortex was also of significant importance in developing higher stresses and displacements. The effects were even more dramatic in the non-uniform loadcase in which maximum displacement was increased by 83% and principal stresses by 92%. Von Mises stresses were also higher by 80%. In the uniform loadcase the corresponding percentages were lower but still significantly large. The fact that part of the anterior cortical shell was degenerated in combination with the increased pressure applied on the anterior part in the non-uniform loadcase, lead to major increases in the observed stresses. Hence, this specific kind of metastatic defects was also one of the most influential in the strength of the vertebral body.

Chapter 5

CONCLUSION

The objectives of this study were achieved and the importance of the various geometric and material property parameters was determined. In developing the models it was found that the biconcavity of the endplate was the most important geometric factor influencing the mechanical behavior of the vertebral body. The effects of osteoporosis, that was modeled as a reduction in the material properties of both cancellous and cortical bone, were also examined and analyzed and found to be critical for the vertebral body. Also the parametric study of metastatic defects was highly successful since a relative order of significance was obtained for the two parameters; size was more important than location. However, the results would have been more enlightening if a larger number of sphere sizes had been examined as well as of locations. Also a conclusion about the relative importance of cancellous and cortical bone in supporting loads would have been reached if models with the same amount of reduction for both types of bone had been utilized. Finally, a model that would include both osteoporosis and a metastatic defect would have been an interesting situation in which we could examine the way in which the two pathological cases combine.

References

[1] Ellis Barnett, B.E.C Nordin.
The Radiological Diagnosis of Osteoporosis:a new approach.
British Journal of Radiology , April, 1968pp.234-241.

[2] A.Nachemson.
The load on Lumbar Disks in Different Positions of the Body.
Clinical Orthopaedics , 1966.

[3] Manfred Horst, Paul Brinckman.
Measurement of the Distribution of Axial Stress on the End-Plate of the Vertebral Body.
Spine , May/June, 1981.

[4] Ruegsegger, P., Dambacher, M.A, Ruesegger, E., Fischer, J.A., and Anlike, M.
Bone Loss in Premenopausal and Postmenopausal Women.
The Journal of Bone and Joint Surgery , September, 1984.

[5] Broberg, K.B.
On the Mechanical Behavior of Intervertebral Discs.
Spine , Vol.8, 1983.

[6] Kaplan, Frederick S.
Osteoporosis: Pathophysiology and Prevention.
Clinical Symposia (CIBA-GEIGY) , 1987.

[7] Firooznia, Hossein, Rafli, Mahvesh, Golimbu, Cornelia, Schwartz, Melvin S., and Ort,Paul.
Trabecular Mineral Content of the Spine in Women with Hip fracture:CT Measurements.
Radiology , Vol. 159, 1986.

[8] Hakim, Nabil S. and King, Albert I.
A Three Dimensional Finite Element Dynamic Response Analysis of a Vertebra with Experimental Verification.
Journal of Biomechanics (12), 1979.

[9] Murray, Pepper R., and Hayes, W.C.
Mechanical properties of the Subchondrial Plate and the Metaphyseal Shell.
M.D. Thesis, Harvard Medical School Class of 1986 , .

[10] Knopf, Kevin.
Analysis of Lumbar Vertebral Strength using a Finite Element Model.
Bachelor Thesis, MIT , May, 1988.

[11] S.M lang, D.D Moyle, Clemson, E.W.Berg, N.Detorie, A.T.Gilpin, N.J. Pappas,JR, J.C. Reynolds, M.Tkacik, R.L.Waldron,II.
Correlation of Mechanical Properties of Vertebral Trabecular Bone with Equivalent Mineral Density as Measured by Computer Tomography.
The journal of Bone and Joint Surgery , Vol.70-A, 1988.

[12] Jeffrey C. Lotz, Tobin N. Gerhart and Wilson C. Hayes.
Mechanical Properties of Trabecular Bone from the Proximal Femur:A Quantitative CT study.
Journal of Computer Assisted Tomography, 1985.

[13] Murray, R.P., Hayes, W.C., Edwards, W.T., and Henry, J.D.,
Mechanical Properties of the Subchondral Plate and Metaphyseal Shell.
ORS 9, Vol.197, 1984.

[14] M.Nissan, I. Gilad.
The cervical and lumbar vertebrae-an anthropometric model.
Engineering in Medicine, Vol.13, 1984.

[15] Moshe Nissan, Issachar Gilad.
Dimensions of Human Lumbar Vertebrae in the Sagittal plane.
Journal of Biomechanics, Vol.19, pp.753-758.

[16] Gerard J. Tortora.
Principles of Human Anatomy.
Harper & Row, Publishers, 1989.

[17] Reinbold, Wolf-Dieter, Genant, Harry K., Reiser, Ulrich J., Harris, Steven T., and Ettinger, Bruce.
Bone Mineral Content in Early Postmenopausal and Postmenopausal Osteoporotic Women: Comparison of Measurement Methods.
Radiology, Vol.160,1986.

[18] Shirazi, Adl, A.,Ahmed,A.M., and Shrivastava,S.C.
A Finite Element Study of a Lumbar Motion Segment Subjected to Pure Sagital Plane Moments.
Journal of Biomechanics, Vol19, 1986.

[19] Yang, K.H., Khalil, T., Tzeng, C.R., and King, A.I.
Finite Element Model of a Functional Spinal Unit.
American Society of Mechanical Engineers Biomechanics Symposium, 1983.

Chapter 6

APPENDIX

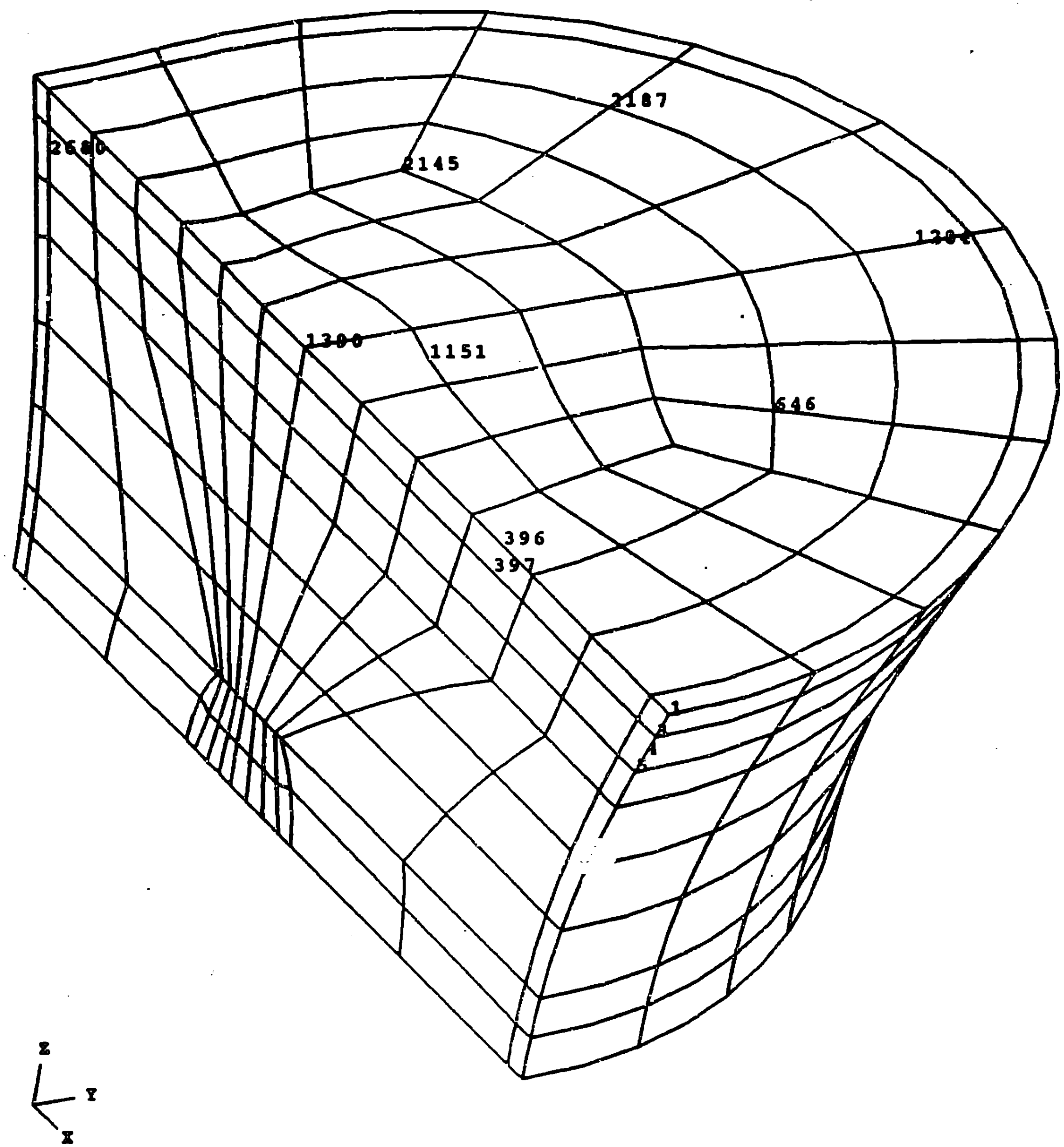

LOCATION OF THE NODES SELECTED FOR THE STUDY

```
C
C     CHANGE2 recalculates the nodal coordinates
C     in order for a tapered and a teardrop cross
C     sectional geometry to be produced
C     SP.NONO3 is the old nodal point file and
C     SP.NONO is the newly generated file
C
C
C
      PI=3.14159
C
C     A=Amplitude of cosine wave which weaves about
C     point B such that A+B=19.55
      A=3.91
      B=15.64
      OPEN (UNIT=1,NAME='SP.NONO3',TYPE='OLD',READONLY)
      OPEN (UNIT=2,NAME='SP.NONO',TYPE='NEW')
 90   READ (1,100) CT,N,JPR,I1,I2,I3,I4,I5,I6,X,Y,Z,KN,NRST,MIDS
100   FORMAT (A1,I4,A1,I4,5I5,3F10.4,3I5)
      TH=ABS(Z*PI)/27.9
      RNEW=A*(1-COS(TH))+B
      IF (X.EQ.0) THEN
         PHI=PI/2
      ELSE IF ((X.LT.0).AND.(Y.EQ.0)) THEN
         PHI=PI
      ELSE IF (X.LT.0) THEN
         PHI=PI-ATAN(ABS(Y/X))
      ELSE IF ((X.GT.0).AND.(Y.GT.0)) THEN
         PHI=ATAN(ABS(Y/X))
      ELSE IF ((X.GT.0).AND.(Y.EQ.0)) THEN
         PHI=0
      ENDIF
      RTEAR=RNEW*(1+0.0649*(COS(PHI)-2*COS(2*PHI)+COS(3*PHI)))
      ZN=Z
      IF (X.NE.0) THEN
      XN=(RTEAR/19.55)*X
      ELSE IF (X.EQ.0) THEN
      XN=0
      ENDIF
      IF (Y.NE.0) THEN
      YN=(RTEAR/19.55)*Y
      ELSE IF (Y.EQ.0) THEN
      YN=0
      ENDIF
      WRITE (2,200) CT,N,JPR,I1,I2,I3,I4,I5,I6,XN,YN,ZN
200   FORMAT (A1,I4,A1,I4,5I5,3F10.4,3I5)
      YO=PHI*(180/PI)
      BO=RTEAR/RNEW
      WRITE (6,300) YO,BO,ZN
300   FORMAT (3F10.4)
      IF (N.LT.1298) GO TO 90
      CLOSE (UNIT=1)
      CLOSE (UNIT=2)
      END
```

```
C
C
C
C      I-N INTEGER, A-J REAL
C      Program CHANGE3 changes mesh to conform
C      to a new geometry that considers
C      biconcavity of the endplate
C      SP.NODO is the old nodal point file and
C      SP.NONO3 is the newly generated file
       PI=3.14159
C
C
       A=1.81
       B=12.14
       OPEN (UNIT=1,NAME='SP.NODO',TYPE='OLD',READONLY)
       OPEN (UNIT=2,NAME='SP.NONO3',TYPE='NEW')
  90   READ (1,100) CT,N,JPR,I1,I2,I3,I4,I5,I6,X,Y,Z,KN,NRST,MIDS
 100   FORMAT (A1,I4,A1,I4,5I5,3F10.4,3I5)
       TH=SQRT(X*X+Y*Y)/39.8*PI
       RNEW=A*(ABS(1-COS(TH)))+B
       XN=X
       YN=Y
       ZN=(RNEW/13.95)*Z
       WRITE (2,200) CT,N,JPR,I1,I2,I3,I4,I5,I6,XN,YN,ZN
 200   FORMAT (A1,I4,A1,I4,5I5,3F10.4,3I5)
       WRITE (6,300) RNEW,TH
 300   FORMAT (2F10.4)
       IF (N.LT.1298) GO TO 90
       CLOSE (UNIT=1)
       CLOSE (UNIT=2)
       END
```

PNT P1	0.00000	0.00000	0.00000
PNT P2	3.30000	0.00000	0.00000
PNT P3	0.00000	3.30000	0.00000
PNT P4	2.48000	2.48000	0.00000
PNT P5	4.13000	0.00000	0.00000
PNT P6	0.00000	4.13000	0.00000
PNT P7	0.00000	0.00000	2.66000
PNT P8	2.07000	0.00000	2.66000
PNT P9	0.00000	2.07000	2.66000
PNT P10	1.65000	1.65000	2.66000
PNT P11	2.48000	0.00000	2.66000
PNT P12	0.00000	2.48000	2.66000
PNT P13	0.00000	0.00000	9.96000
PNT P14	0.00000	9.09000	9.96000
PNT P15	9.09000	0.00000	9.96000
PNT P16	7.44000	7.44000	9.96000
PNT P17	18.90000	0.00000	0.00000
PNT P18	0.00000	18.90000	0.00000
PNT P19	18.90000	0.00000	2.66000
PNT P20	0.00000	18.90000	2.66000
PNT P21	18.90000	0.00000	9.96000
PNT P22	0.00000	18.90000	9.96000
PNT P23	19.90000	0.00000	0.00000
PNT P24	0.00000	19.90000	0.00000
PNT Q1	19.90000	0.00000	2.66000
PNT Q2	0.00000	19.90000	2.66000
PNT Q3	19.90000	0.00000	9.96000
PNT Q4	0.00000	19.90000	9.96000
PNT Q5	0.00000	9.09000	12.95000
PNT Q6	7.44000	7.44000	12.95000
PNT Q7	9.09000	0.00000	12.95000
PNT Q8	0.00000	0.00000	12.95000
PNT Q9	0.00000	18.90000	12.95000
PNT Q10	18.90000	0.00000	12.95000
PNT Q11	19.90000	0.00000	12.95000
PNT Q12	0.00000	19.90000	12.95000
PNT Q13	0.00000	9.09000	13.95000
PNT Q14	7.44000	7.44000	13.95000
PNT Q15	9.09000	0.00000	13.95000
PNT Q16	0.00000	0.00000	13.95000
PNT Q17	0.00000	18.90000	13.95000
PNT Q18	18.90000	0.00000	13.95000
PNT Q19	19.90000	0.00000	13.95000
PNT Q20	0.00000	19.90000	13.95000
PNT P25	-7.44000	7.44000	9.96000
PNT Q21	-2.07000	0.00000	2.66000
PNT Q22	-1.65000	1.65000	2.66000
PNT Q23	-3.30000	0.00000	0.00000
PNT Q24	-2.48000	2.48000	0.00000
PNT Q25	-2.48000	0.00000	2.66000
PNT Q26	-4.13000	0.00000	0.00000
PNT Q27	-7.44000	0.00000	9.96000
PNT Q28	-18.90000	0.00000	9.96000
PNT Q29	-18.90000	0.00000	2.66000
PNT Q30	-18.90000	0.00000	0.00000
PNT Q31	-19.90000	0.00000	0.00000
PNT Q32	-19.90000	0.00000	2.66000
PNT Q33	-19.90000	0.00000	9.66000
PNT Q34	-7.44000	7.44000	12.95000
PNT Q35	-9.09000	0.00000	12.95000
PNT Q36	-18.90000	0.00000	12.95000
PNT Q37	-19.90000	0.00000	12.95000
PNT Q38	-7.44000	7.44000	13.95000
PNT Q39	-9.09000	0.00000	13.95000
PNT Q40	-18.90000	0.00000	13.95000
PNT Q41	-19.90000	0.00000	13.95000

```
LINE L1    P1    P2          6
LINE L2    P1    P3          6
LINE L3    P3    P4          6
LINE L4    P4    P2          6
LINE L5    P2    P5          2
LINE L6    P3    P6          2
LINE C7    P5    P6    P1          12
LINE L8    P7    P8          6
LINE L9    P7    P9          6
LINE L10   P9    P10         6
LINE L11   P10   P8          6
LINE L12   P8    P11         2
LINE L13   P9    P12         2
LINE C14   P11   P12   P7          12
LINE C15   P5    P11   P1           4
LINE C16   P6    P12   P1           4
LINE L17   P1    P7          4
LINE L18   P2    P8          4
LINE L19   P4    P10         4
LINE L20   P3    P9          4
LINE L21   P7    P13         6
LINE L22   P9    P14         6
LINE L23   P10   P16         6
LINE L24   P8    P15         6
LINE L25   P13   P14         6
LINE L26   P14   P16         6
LINE L27   P16   P15         6
LINE L28   P15   P13         6
LINE C29   P17   P18   P1          12
LINE C30   P20   P19   P7          12
LINE C31   P22   P21   P13         12
LINE L32   P14   P22         6
LINE L33   P15   P21         6
LINE L34   P12   P20         4
LINE L35   P11   P19         4
LINE L36   P18   P6          4
LINE L37   P17   P5          4
LINE L38   P22   P20         6
LINE L39   P21   P19         6
LINE L40   P20   P18         4
LINE L41   P19   P17         4
LINE C42   P23   P24   P1          12
LINE L43   P18   P24         2
LINE L44   P17   P23         2
LINE U1    P23   Q1          4
LINE U2    P24   Q2          4
LINE U3    Q1    Q2    P7          12
LINE U4    P20   Q2          2
LINE U5    P19   Q1          2
LINE U6    Q1    Q3          6
LINE U7    Q2    Q4          6
LINE U8    Q3    Q4    P13         12
LINE U9    P22   Q4          2
LINE U10   P21   Q3          2
LINE U11   P14   Q5          4
LINE U12   P16   Q6          4
LINE U13   Q5    Q6          6
LINE U14   P15   Q7          4
LINE U15   Q6    Q7          6
LINE U16   P13   Q8          4
LINE U17   Q7    Q8          6
LINE U18   Q8    Q5          6
LINE U20   P22   Q9          4
LINE U21   Q5    Q9          6
LINE U22   P21   Q10         4
LINE U23   Q9    Q10   Q8          12
```

```
LINE U24   Q7    Q10         6
LINE U25   Q3    Q11         4
LINE U26   Q4    Q12         4
LINE U27   Q11   Q12   Q8          12
LINE U28   Q9    Q12         2
LINE U29   Q10   Q11         2
LINE U30   Q5    Q13         2
LINE U31   Q6    Q14         2
LINE U32   Q13   Q14         6
LINE U33   Q7    Q15         2
LINE U34   Q14   Q15         6
LINE U35   Q8    Q16         2
LINE U36   Q15   Q16         6
LINE U37   Q16   Q13         6
LINE U39   Q9    Q17         2
LINE U40   Q13   Q17         6
LINE U41   Q10   Q18         2
LINE U42   Q17   Q18   Q16         12
LINE U43   Q15   Q18         6
LINE U44   Q11   Q19         2
LINE U45   Q12   Q20         2
LINE U46   Q19   Q20   Q16         12
LINE U47   Q17   Q20         2
LINE U48   Q18   Q19         2
LINE U49   P7    Q21         6
LINE U50   P9    Q22         6
LINE U51   Q22   Q21         6
LINE U52   P1    Q23         6
LINE U53   P3    Q24         6
LINE U54   Q24   Q23         6
LINE U55   Q23   Q21         4
LINE U56   Q24   Q22         4
LINE U58   Q21   Q25         2
LINE U59   Q25   P12   P7          12
LINE U61   Q23   Q26         2
LINE U62   Q26   P6    P1          12
LINE U63   Q26   Q25   P1           4
LINE U64   P14   P25         6
LINE U65   P25   Q27         6
LINE U66   Q27   P13         6
LINE U67   Q22   P25         6
LINE U68   Q21   Q27         6
LINE U70   P22   Q28   P13         12
LINE U71   Q28   Q29         6
LINE U72   P20   Q29   P7          12
LINE U73   Q27   Q28         6
LINE U74   Q25   Q29         4
LINE U76   Q29   Q30         4
LINE U77   Q30   P18   P1          12
LINE U78   Q30   Q26         4
LINE U79   Q31   P24   P1          12
LINE U80   Q30   Q31         2
LINE U81   Q32   Q2    P7          12
LINE U82   Q29   Q32         2
LINE U83   Q31   Q32         4
LINE U84   Q33   Q4    P13         12
LINE U85   Q28   Q33         2
LINE U86   Q32   Q33         6
LINE U87   Q5    Q34         6
LINE U88   Q34   Q35         6
LINE U89   Q35   Q8          6
LINE U90   P25   Q34         4
LINE U91   Q27   Q35         4
LINE U93   Q9    Q36   Q8          12
LINE U94   Q35   Q36         6
LINE U95   Q28   Q36         4
```

```
LINE U96   Q37   Q12   Q8        12
LINE U97   Q36   Q37         2
LINE U98   Q33   Q37         4
LINE U99   Q13   Q38         6
LINE U100  Q38   Q39         6
LINE U101  Q39   Q16         6
LINE U102  Q34   Q38         2
LINE U103  Q35   Q39         2
LINE U105  Q17   Q40   Q16       12
LINE U106  Q39   Q40         6
LINE U107  Q36   Q40         2
LINE U108  Q41   Q20   Q16       12
LINE U109  Q40   Q41         2
LINE U110  Q37   Q41         2
LCMB LC1   L3    L4
LCMB LC2   L10   L11
LCMB LC3   L26   L27
LCMB LC4   L34   L13
LCMB LC5   L35   L12
LCMB U19   U13   U15
LCMB U38   U32   U34
LCMB U57   U50   U51
LCMB U60   U53   U54
LCMB U69   U64   U65
LCMB U75   U74   U58
LCMB U92   U87   U88
LCMB U104  U99   U100
SURF S1    L1    L2    L3    L4
SURF S2    L8    L9    L10   L11
SURF S3    L18   L4    L19   L11
SURF S4    L19   L3    L20   L10
SURF S5    L20   L9    L17   L2
SURF S6    L17   L8    L18   L1
SURF S7    LC1   L5    C7    L6
SURF S8    LC2   L12   C14   L13
SURF S9    L18   L12   C15   L5
SURF S10   C15   C7    C16   C14
SURF S11   C16   L13   L20   L6
SURF S12   L20   LC2   L18   LC1
SURF S13   L25   L22   L9    L21
SURF S14   L26   L23   L10   L22
SURF S15   L24   L27   L23   L11
SURF S16   L28   L24   L8    L21
SURF S17   L26   L27   L28   L25
SURF S18   L38   C31   L39   C30
SURF S19   L38   L32   L22   LC4
SURF S20   L24   L33   L39   LC5
SURF S21   LC3   L32   C31   L33
SURF S22   LC2   LC4   C30   LC5
SURF S23   L36   L40   L34   C16
SURF S24   L37   L41   L35   C15
SURF S25   L40   C30   L41   C29
SURF S26   LC2   L22   LC3   L24
SURF S27   C29   L36   C7    L37
SURF S28   L35   C30   L34   C14
SURF S29   C42   L43   C29   L44
SURF V1    C42   U1    U3    U2
SURF V2    L43   L40   U4    U2
SURF V3    L44   L41   U5    U1
SURF S30   U3    U4    C30   U5
SURF V4    U3    U6    U8    U7
SURF V5    U4    L38   U9    U7
SURF V6    U5    L39   U10   U6
SURF S31   U8    U9    C31   U10
SURF V7    L26   U11   U13   U12
SURF V8    L27   U12   U15   U14
```

SURF	V9	L28	U14	U17	U16
SURF	V10	L25	U16	U18	U11
SURF	V11	U13	U15	U17	U18
SURF	V12	LC3	U11	U19	U14
SURF	V13	L32	U11	U21	U20
SURF	V14	C31	U20	U23	U22
SURF	V15	L33	U14	U24	U22
SURF	V16	U19	U21	U23	U24
SURF	V17	U8	U25	U27	U26
SURF	V18	U9	U20	U28	U26
SURF	V19	U10	U22	U29	U25
SURF	V20	U27	U28	U23	U29
SURF	V21	U13	U30	U32	U31
SURF	V22	U15	U31	U34	U33
SURF	V23	U17	U33	U36	U35
SURF	V24	U18	U35	U37	U30
SURF	V25	U32	U34	U36	U37
SURF	V26	U19	U30	U38	U33
SURF	V27	U21	U30	U40	U39
SURF	V28	U23	U39	U42	U41
SURF	V29	U24	U33	U43	U41
SURF	V30	U38	U40	U42	U43
SURF	V31	U27	U44	U46	U45
SURF	V32	U28	U39	U47	U45
SURF	V33	U29	U41	U48	U44
SURF	V34	U46	U47	U42	U48
SURF	V35	U49	L9	U50	U51
SURF	V36	U52	L2	U53	U54
SURF	V37	U55	U54	U56	U51
SURF	V38	U56	U53	L20	U50
SURF	V39	L17	U49	U55	U52
SURF	V40	U57	U58	U59	L13
SURF	V41	U60	U61	U62	L6
SURF	V42	U55	U58	U63	U61
SURF	V43	U63	U62	C16	U59
SURF	V44	L20	U57	U55	U60
SURF	V45	U64	U65	U66	L25
SURF	V46	U64	U67	U50	L22
SURF	V47	U68	U65	U67	U51
SURF	V48	U66	U68	U49	L21
SURF	V49	U57	L22	U69	U68
SURF	V50	L38	U70	U71	U72
SURF	V51	U69	L32	U70	U73
SURF	V52	U68	U73	U71	U75
SURF	V53	U57	LC4	U72	U75
SURF	V54	L40	U72	U76	U77
SURF	V55	U74	U72	L34	U59
SURF	V56	U77	L36	U62	U78
SURF	V57	U78	U76	U74	U63
SURF	V58	U79	L43	U77	U80
SURF	V59	U81	U4	U72	U82
SURF	V60	U79	U83	U81	U2
SURF	V61	U80	U76	U82	U83
SURF	V62	U84	U9	U70	U85
SURF	V63	U81	U86	U84	U7
SURF	V64	U82	U71	U85	U86
SURF	V65	U87	U88	U89	U18
SURF	V66	U64	U11	U87	U90
SURF	V67	U65	U90	U88	U91
SURF	V68	U66	U91	U89	U16
SURF	V69	U92	U21	U93	U94
SURF	V70	U69	U11	U92	U91
SURF	V71	U70	U20	U93	U95
SURF	V72	U73	U91	U94	U95
SURF	V73	U96	U28	U93	U97
SURF	V74	U84	U98	U96	U26

```
SURF V75  U85  U95  U97  U98
SURF V76  U99  U100 U101 U37
SURF V77  U87  U30  U99  U102
SURF V78  U88  U102 U100 U103
SURF V79  U89  U103 U101 U35
SURF V80  U104 U40  U105 U106
SURF V81  U92  U30  U104 U103
SURF V82  U93  U39  U105 U107
SURF V83  U94  U103 U106 U107
SURF V84  U108 U47  U105 U109
SURF V85  U96  U110 U108 U45
SURF V86  U97  U107 U109 U110
BODY W1   S2   S1   S3   S4   S5   S6
BODY W2   S8   S7   S9   S10  S11  S12
BODY W3   S17  S2   S14  S15  S16  S13
BODY W4   S26  S18  S19  S21  S20  S22
BODY W5   S10  S25  S28  S23  S27  S24
BODY W6   S29  S30  V1   V2   S25  V3
BODY W7   S30  S31  V4   V5   S18  V6
BODY W8   S17  V11  V7   V8   V9   V10
BODY W9   S21  V16  V12  V13  V14  V15
BODY W10  S31  V20  V17  V18  V14  V19
BODY W11  V11  V25  V21  V22  V23  V24
BODY W12  V16  V30  V26  V27  V28  V29
BODY W13  V20  V34  V31  V32  V28  V33
BODY W14  V35  V36  V37  V38  S5   V39
BODY W15  V40  V41  V42  V43  S11  V44
BODY W16  V45  V35  V46  V47  V48  S13
BODY W17  V49  V50  S19  V51  V52  V53
BODY W18  V43  V54  V55  S23  V56  V57
BODY W19  V58  V59  V60  V2   V54  V61
BODY W20  V59  V62  V63  V5   V50  V64
BODY W21  V45  V65  V66  V67  V68  V10
BODY W22  V51  V69  V70  V13  V71  V72
BODY W23  V62  V73  V74  V18  V71  V75
BODY W24  V65  V76  V77  V78  V79  V24
BODY W25  V69  V80  V81  V27  V82  V83
BODY W26  V73  V84  V85  V32  V82  V86
ELTY S1   QU8       1
ELTY S2   QU8       1
ELTY S3   QU8       1
ELTY S4   QU8       1
ELTY S5   QU8       1
ELTY S6   QU8       1
ELTY S7   QU8       1
ELTY S8   QU8       1
ELTY S9   QU8       1
ELTY S10  QU8       1
ELTY S11  QU8       1
ELTY S12  QU8       1
ELTY S13  QU8       1
ELTY S14  QU8       1
ELTY S15  QU8       1
ELTY S16  QU8       1
ELTY S17  QU8       1
ELTY S18  QU8       1
ELTY S19  QU8       1
ELTY S20  QU8       1
ELTY S21  QU8       1
ELTY S22  QU8       1
ELTY S23  QU8       1
ELTY S24  QU8       1
ELTY S25  QU8       1
ELTY S26  QU8       1
ELTY S27  QU8       1
ELTY S28  QU8       1
```

ELTY	S29	QU8	1
ELTY	V1	QU8	1
ELTY	V2	QU8	1
ELTY	V3	QU8	1
ELTY	S30	QU8	1
ELTY	V4	QU8	1
ELTY	V5	QU8	1
ELTY	V6	QU8	1
ELTY	S31	QU8	1
ELTY	V7	QU8	1
ELTY	V8	QU8	1
ELTY	V9	QU8	1
ELTY	V10	QU8	1
ELTY	V11	QU8	1
ELTY	V12	QU8	1
ELTY	V13	QU8	1
ELTY	V14	QU8	1
ELTY	V15	QU8	1
ELTY	V16	QU8	1
ELTY	V17	QU8	1
ELTY	V18	QU8	1
ELTY	V19	QU8	1
ELTY	V20	QU8	1
ELTY	V25	QU8	1
ELTY	V30	QU8	1
ELTY	V34	QU8	1
ELTY	V35	QU8	1
ELTY	V36	QU8	1
ELTY	V37	QU8	1
ELTY	V38	QU8	1
ELTY	V39	QU8	1
ELTY	V40	QU8	1
ELTY	V41	QU8	1
ELTY	V42	QU8	1
ELTY	V43	QU8	1
ELTY	V44	QU8	1
ELTY	V45	QU8	1
ELTY	V46	QU8	1
ELTY	V47	QU8	1
ELTY	V48	QU8	1
ELTY	V49	QU8	1
ELTY	V50	QU8	1
ELTY	V51	QU8	1
ELTY	V52	QU8	1
ELTY	V53	QU8	1
ELTY	V54	QU8	1
ELTY	V55	QU8	1
ELTY	V56	QU8	1
ELTY	V57	QU8	1
ELTY	V58	QU8	1
ELTY	V59	QU8	1
ELTY	V60	QU8	1
ELTY	V61	QU8	1
ELTY	V62	QU8	1
ELTY	V63	QU8	1
ELTY	V64	QU8	1
ELTY	V65	QU8	1
ELTY	V66	QU8	1
ELTY	V67	QU8	1
ELTY	V68	QU8	1
ELTY	V69	QU8	1
ELTY	V70	QU8	1
ELTY	V71	QU8	1
ELTY	V72	QU8	1
ELTY	V73	QU8	1
ELTY	V74	QU8	1

```
ELTY V75  QU8    1
ELTY V76  QU8    1
ELTY V80  QU8    1
ELTY V84  QU8    1
ELTY W1   HE20   1
ELTY W2   HE20   1
ELTY W3   HE20   1
ELTY W4   HE20   1
ELTY W5   HE20   1
ELTY W6   HE20   1
ELTY W7   HE20   1
ELTY W8   HE20   1
ELTY W9   HE20   1
ELTY W10  HE20   1
ELTY W11  HE20   1
ELTY W12  HE20   1
ELTY W13  HE20   1
ELTY W14  HE20   1
ELTY W15  HE20   1
ELTY W16  HE20   1
ELTY W17  HE20   1
ELTY W18  HE20   1
ELTY W19  HE20   1
ELTY W20  HE20   1
ELTY W21  HE20   1
ELTY W22  HE20   1
ELTY W23  HE20   1
ELTY W24  HE20   1
ELTY W25  HE20   1
ELTY W26  HE20   1
SETA SE1  S17  S21  S31
SETA SE2  Q13  Q14  Q15  Q16  Q17  Q18  Q19  Q20  U30  U31  U32  U33  U34
          ,    U35  U36  U37  U38  U39  U40  U41  U42  U43  U44  U45  U46  U47
          ,    U48  V11  V16  V20  V21  V22  V23  V24  V25  V26  V27  V28  V29
          ,    V30  V31  V32  V33  V34  W11  W12  W13
SETA SE3  S1   S7
SETA SE4  S2   S8
SETA SE8  V25  V30  V34
SETA SE5  W1   W2   W3   W4   W5   W6   W7   W8   W9   W10  W11  W12  W13
SETA SE6  W14  W15  W16  W17  W18  W19  W20  W21  W22  W23  W24  W25  W26
SETA SE7  W1   W2   W3   W4   W5   W6   W7   W8   W9   W10  W11  W12  W13
          ,    W14  W15  W16  W17  W18  W19  W20  W21  W22  W23  W24  W25  W26
```